Electronic Supplementary Material (ESI) for Nanoscale.

Supporting Information

Polymeric architecture as a tool for controlling the reactivity of palladium (II) loaded nanoreactors.

Shreyas S. Wagle [1,2], Parul Rathee [1,2], Krishna Vippala [1,2,3], Shahar Tevet [1,2], Alexander Gordin [4] Roman Dobrovetsky [1], Roey J. Amir* [1,2,4,5]

1. *Department of Organic Chemistry, School of Chemistry, Faculty of Exact Sciences, Tel-Aviv University, Tel-Aviv 6997801, Israel.*
2. *Tel-Aviv University Center for Nanoscience and Nanotechnology, Tel-Aviv University, Tel-Aviv, 6997801, Israel.*
3. *Analytical Technologies Unit R&D, Teva Pharmaceutical Industries, Kfar Saba 4410202, Israel.*
4. *The ADAMA Center for Novel Delivery Systems in Crop Protection, Tel-Aviv University, Tel-Aviv, 6997801, Israel.*
5. *The Center for Physics and Chemistry of Living Systems, Tel-Aviv University, Tel-Aviv 6997801, Israel.*

Table of Contents

1. Instrumentation and Materials

1.1. Instrumentation

HPLC: All measurements were recorded on a Waters Alliance e2695 separations module equipped with a Waters 2998 photodiode array detector. All solvents were purchased from Bio-Lab Chemicals and were used as received. All solvents are HPLC grade.

^{1}H and ^{13}C NMR: Spectra were recorded on Bruker Avance I and Avance III 400MHz/100MHz spectrometer as indicated. Chemical shifts are reported in ppm and referenced to the solvent.

GPC: All measurements were recorded on Viscotek GPCmax by Malvern using refractive index detector and PEG standards (purchased from Sigma-Aldrich) were used for calibration. DMF (purchased from Sigma, HPLC grade) was used as mobile phase. Columns (2 x PSS GRAM 1000Å) were used at a column temperature of 50°C.

Fluorescence spectra: CMC measurements were recorded on a TECAN Infinite M200Pro device; anisotropy measurements were recorded on an Agilent Technologies Cary Eclipse Fluorescence Spectrometer using quartz cuvettes along with 50.8 mm x 50.8 mm economy visible light linear polarizers from Thorlabs.

LC-MS: Measurements were conducted on a LCMS Xevo–TQD and analysis on Agilent 1260 system with single quadrupole MSD featured with multimode (ESI+APCI) ionization chamber.

TEM: Images were taken by a JEM-1400Plus at 80 kV.

DLS: All measurements were recorded on a Corduan Technology VASCOγ particle size analyzer.

ICP-MS: Measurements were conducted on Agilent 7800 ICP-MS equipped with SPS4 Autosampler.

Simulation: Density functional theory (DFT) calculations at BP86-D3/def2SVP with SDD on Palladium.

1.2. Materials

Poly (Ethylene Glycol) methyl ether (M_n=5kDa), 2,2-dimethoxy-2-phenylacetophenone (DMPA, 99%), allyl bromide (99%), propargyl bromide (80% in toluene), 4-Nitrophenol (99.5%), 4-Nitroaniline (99.5%), 1-undecanethiol (98 %), 1-tetradecanethiol (98 %), palladium acetate (98%) and Sephadex® LH20 were purchased from Sigma-Aldrich. Cysteamine hydrochloride (98%), potassium hydroxide, Oxyma Pure and Diisopropylethylamine (DIPEA) (99%) were purchased from Merck. 1-hexanethiol (96%), 1-heptanethiol (98%) and 3,4-dihydroxy benzoic acid (97%) were purchased from Alfa Aesar. 3,5 dihydroxy benzoic acid (97%) was purchased from Apollo Scientific Ltd. N,N′-Diisopropylcarbodiimide (DIC) (98%) was purchased from Tzamal

Chem. Azobisisobutyronitrile (AIBN) was purchased from Glentham Life Sciences. 3,4,5-trihydroxy benzoic acid (98%) was purchased from Chem-Impex. Anhydrous potassium carbonate (K_2CO_3) was purchased from J. T. Baker. Anhydrous Na_2SO_4 (granular, 10-60mesh) was purchased from Macron. Silica Gel 60Å, 0.040-0.063 mm, sodium hydroxide and all solvents were purchased from Bio-Lab and were used as received. Deuterated solvents for NMR were purchased from Cambridge Isotope Laboratories (CIL), Inc.

2. Synthesis

Synthesis of the $mPEG_{5k}$-D-$(CX)_3$, $mPEG_{5k}$-D-$(CX)_4$ and $mPEG_{5k}$-D-$(CX)_6$ polymers:

$mPEG_{5k}$-NH_2, $mPEG_{5k}$-triene and $mPEG_{5k}$-diyne were synthesized as previously reported[1] and the spectroscopic characterization correlated well with these reports.

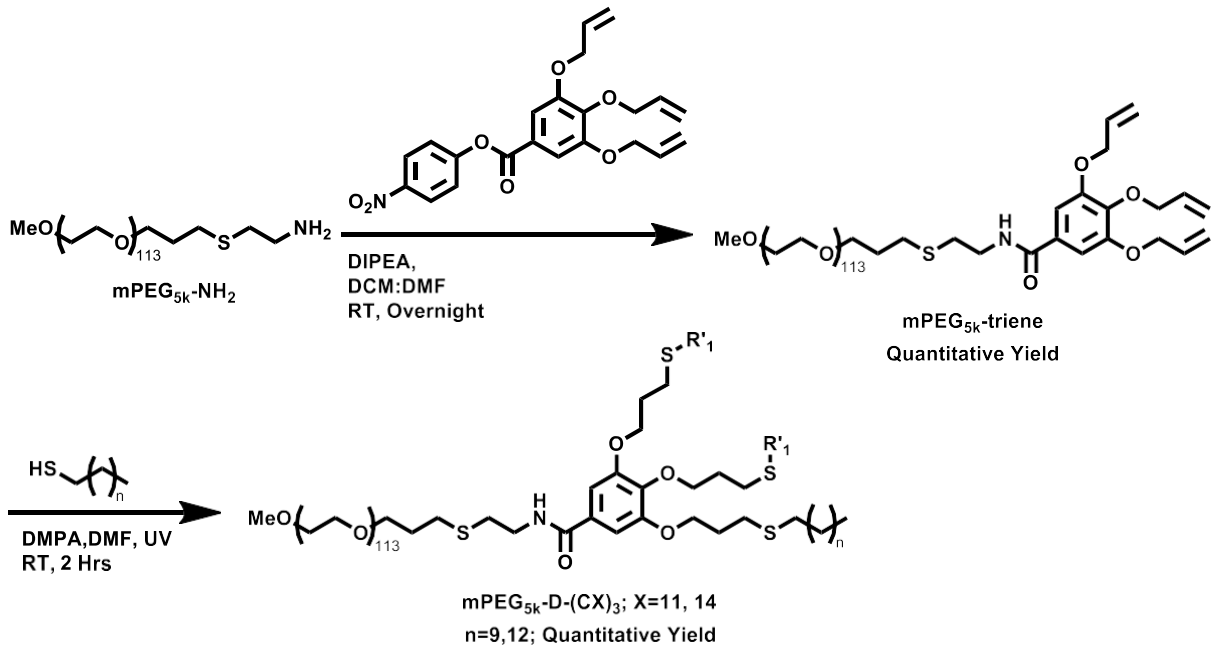

Figure S1: Synthesis of $mPEG_{5k}$-D-$(CX)_3$ amphiphile.

For making the three-armed amphiphile, $mPEG_{5k}$-triene (90 mg, 0.0167 mmol), 1-tetradecanethiol (188 mg, 224 µL, 60 eq, 1 mmol) /1-undecanethiol (230 mg, 272 µL, 60 eq, 1 mmol) and DMPA (3 mg, 0.6 eq., 0.01 mmol; 1 mol% with respect to the thiol) were dissolved in DMF (0.5 mL per 100 mg of hybrid). The solution was purged with nitrogen for 20 minutes and then stirred under UV light (365 nm) for 2 hours. Then, the reaction mixture was loaded as-is on a MeOH-based LH20 (Sephadex®) size exclusion column. Fractions that contained the product (identified by UV light and/or coloring with iodine) were unified, the organic solvents were evaporated to dryness

and the white solid was dried under high vacuum to give the final amphiphiles quantitative yields (99mg).

^{1}H-NMR (400 MHz, Chloroform-d): δ 7.00 (s, 2H, Ar-***H***), 6.63 (t, *J*=5.7 Hz, 1H, -N***H***-CO-), 4.25-4.03 (m, 6H, Ar-O-C***H***$_2$-), 3.85-3.42 (m, PEG backbone), 3.37 (s, 3H, ***H***$_3$C-O-), 2.82-2.42 (m, 16 H, -S-C***H***$_2$-), 2.22-2.02 (p, 6.5 Hz, 4H, -O-CH$_2$-C***H***$_2$-CH$_2$-S), 1.67-1.49 (m, 6H, -C***H***$_2$-CH$_2$-S-), 1.44-1.16 (m, 48H, -CH$_2$-C***H***$_2$-C***H***$_2$-CH$_2$- + -C***H***$_2$-CH$_3$), 0.87 (t, *J*=7.0 Hz, 9H,-CH$_2$-C***H***$_3$). ^{13}C NMR (100 MHz, Chloroform-d): 167.2, 152.8, 129.9, 122.9, 105.9, 70.7, 67.7, 61.8, 59.1, 39.1, 32.4, 32.3, 32.0, 31.8, 30.6, 29.9, 29.8, 29.7, 29.4, 29.1, 28.9, 28.7, 28.3, 22.8, 14.2. GPC (DMF + 25 mM NH$_4$Ac): expected M$_n$= 6.0 kDa, experimental M$_n$ = 5.7 kDa, Đ = 1.04.

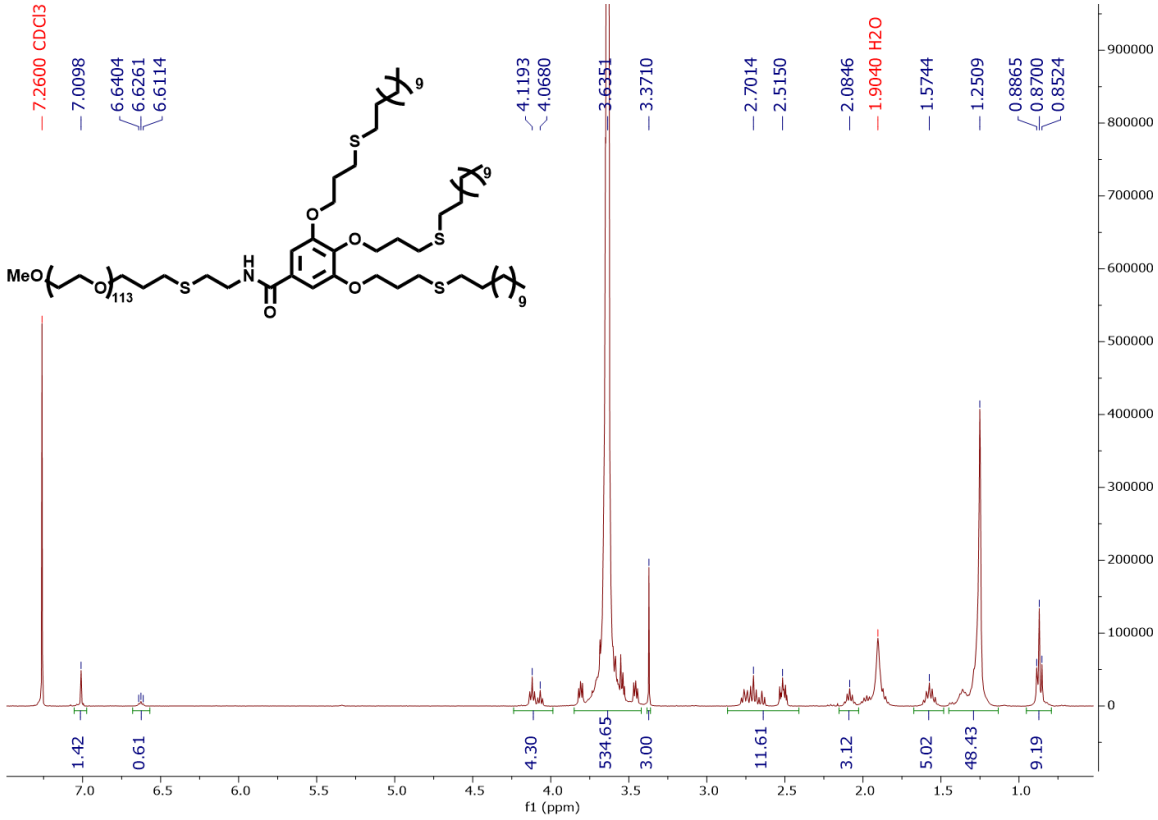

Figure S2: ^{1}H-NMR spectrum of mPEG$_{5k}$-D-(C11)$_3$ (***C11x3***) in CDCl$_3$.

^{1}H-NMR (400 MHz, Chloroform-d): δ 7.01 (s, 2H, Ar-***H***), 6.60 (t, *J*=5.7 Hz, 1H, -N***H***-CO-), 4.06 (m, 6H, Ar-O-C***H***$_2$-), 3.85-3.43 (m, PEG), 3.37 (s, 3H, ***H***$_3$C-O-), 2.85-2.45 (m, 16H, -S-C***H***$_2$-), 1.65-1.51 (m, 6H, -C***H***$_2$-CH$_2$-S-), 1.44-1.16 (m, 66H, -CH$_2$-C***H***$_2$-C***H***$_2$-CH$_2$- + -C***H***$_2$-CH$_3$), 0.87 (t, *J*=7.0 Hz, 9H,-CH$_2$-C***H***$_3$). ^{13}C NMR (100 MHz, Chloroform-d): δ 167.1, 152.8, 140.7, 129.8, 105.9,

70.6, 67.7, 61.7, 59.1, 52.2, 39.1, 32.3, 32.2, 32.0, 31.8, 30.5, 29.7, 29.4, 29.4, 29.1, 29.0, 28.8, 28.7, 28.3, 22.7, 14.2. GPC (DMF + 25 mM NH_4Ac): expected M_n= 6.1 kDa, experimental M_n = 6.3 kDa, Đ = 1.03.

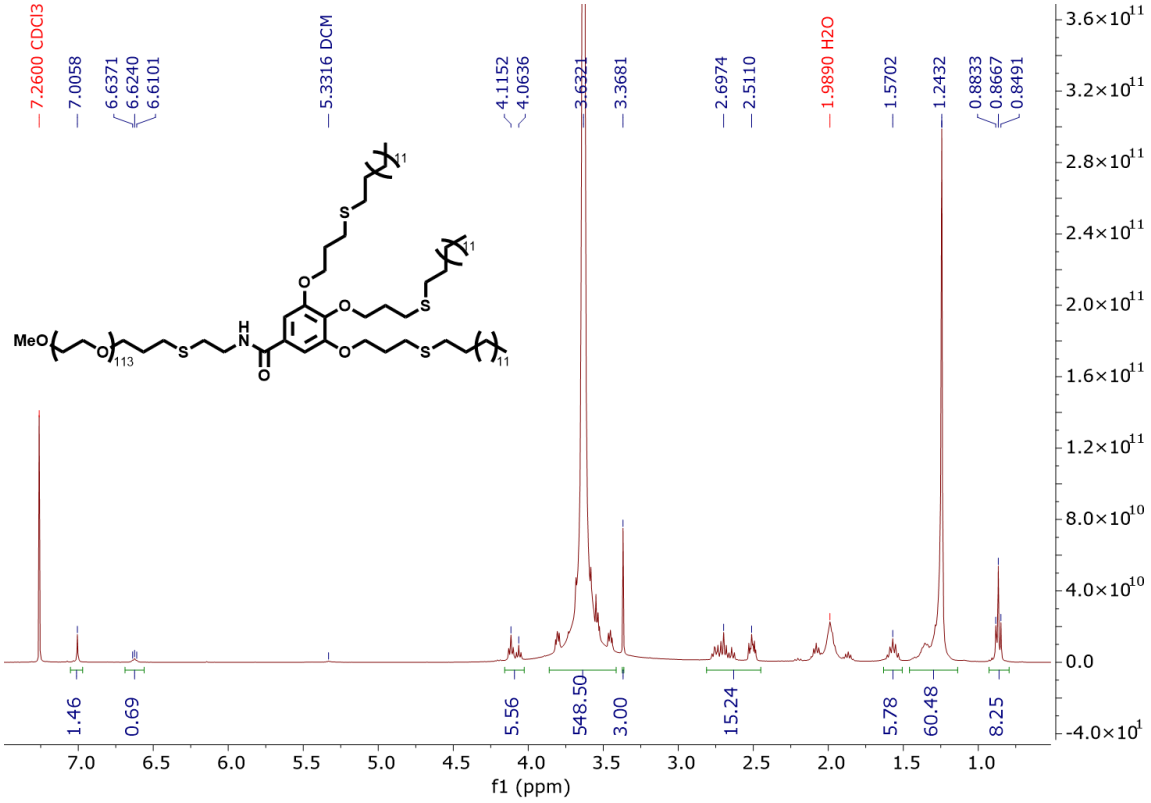

Figure S3: ^{1}H-NMR spectrum of $mPEG_{5k}$-D-$(C14)_3$ (***C14x3***) in $CDCl_3$.

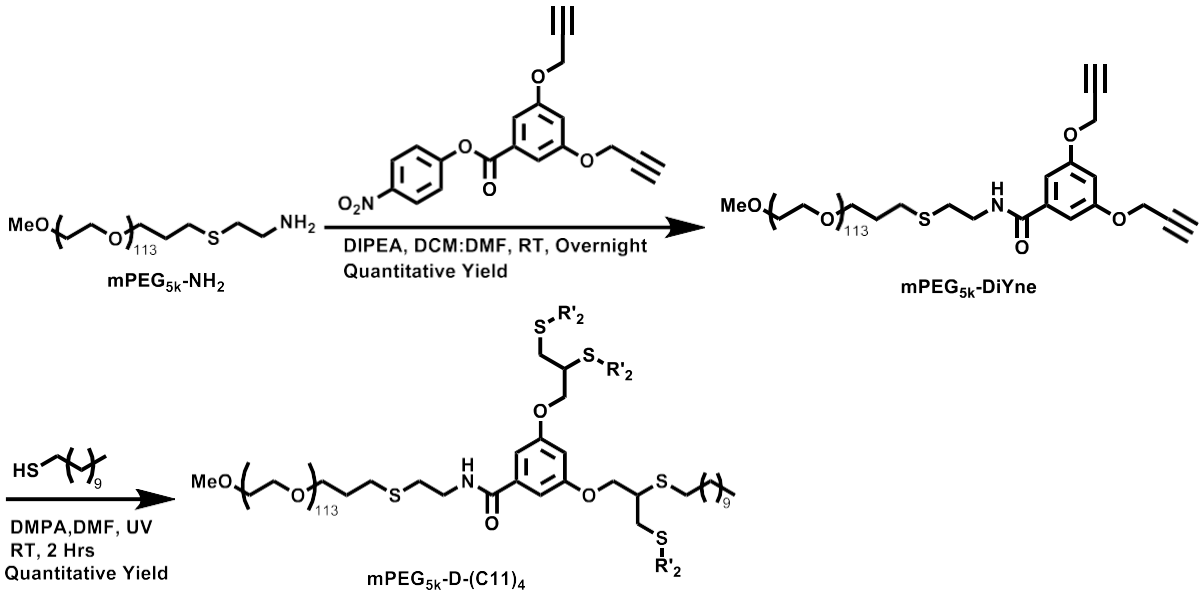

Figure S4: Synthesis of $mPEG_{5k}$-D-$(C11)_4$ (3,5) (***C11x4 (3,5)***) amphiphile.

$mPEG_{5k}$-diyne was synthesized as previously reported.[2]

For making the four-armed C11 [C11x4 (3,5)] amphiphile, $mPEG_{5k}$-diyne (100 mg, 0.0187 mmol), 1-undecanethiol (141 mg, 170 µL, 40 eq. 0.75 mmol) and DMPA (2 mg, 0.4 eq., 0.007 mmol; 1 mol% with respect to the thiol) were dissolved in DMF (0.5 mL per 100 mg of hybrid). The solution was purged with nitrogen for 20 minutes and then stirred under UV light (365 nm) for 2 hours. Then, the reaction mixture was loaded as-is on a MeOH-based LH20 (Sephadex®) size exclusion column. Fractions that contained the product (identified by UV light and/or coloring with iodine) were unified, the organic solvents were evaporated to dryness and the white solid was dried under a high vacuum. The product was obtained in 90 % yield (103 mg).

^{1}H-NMR (400 MHz, Chloroform-d) δ 6.93 (d, *J*=1.72 Hz, 2H, Ar-***H***), 6.60 (m, 2H, -CH-N***H***-CO-Ar- + -Ar-***H***), 4.36–4.04 (m, 4H, -C***H***$_2$-O-Ar), 3.80-3.43 (m, PEG backbone), 3.37 (s, 3H, C***H***$_3$-O-PEG), 3.11 (p, *J* =6.1 Hz, 2H,-C***H***-S-), 3.00– 2.82 (m, 4H, CH_2-C***H***$_2$-S-), 2.76 (t, *J* =6.6 Hz, 2H,-CH_2-C***H***$_2$-S-), 2.69-2.59 (m, 6H,-CH_2-C***H***$_2$-S-), 2.54 (t, *J* =7.5 Hz, 4H,-CH_2-C***H***$_2$-S-), 1.67– 1.51 (m, 8H,-C***H***$_2$-CH_2-S-), 1.47– 1.15 (m, 64H,-CH_2-C***H***$_2$-C***H***$_2$-CH_2- +-C***H***$_2$-CH_3), 0.85 (t, *J* =7.0 Hz, 12H,-CH_2-C***H***$_3$). ^{13}C NMR (100 MHz, Chloroform-d): δ 167.1, 159.9, 136.8, 106.1, 104.7, 70.7, 69.5, 61.8, 59.1, 45.2, 39.0, 34.8, 33.4, 32.0, 29.8, 29.7, 29.3, 28.3, 22.8, 14.2. GPC (DMF + 25 mM NH_4Ac): expected M_n= 6.1 kDa, experimental M_n = 6.3 kDa, Đ = 1.04.

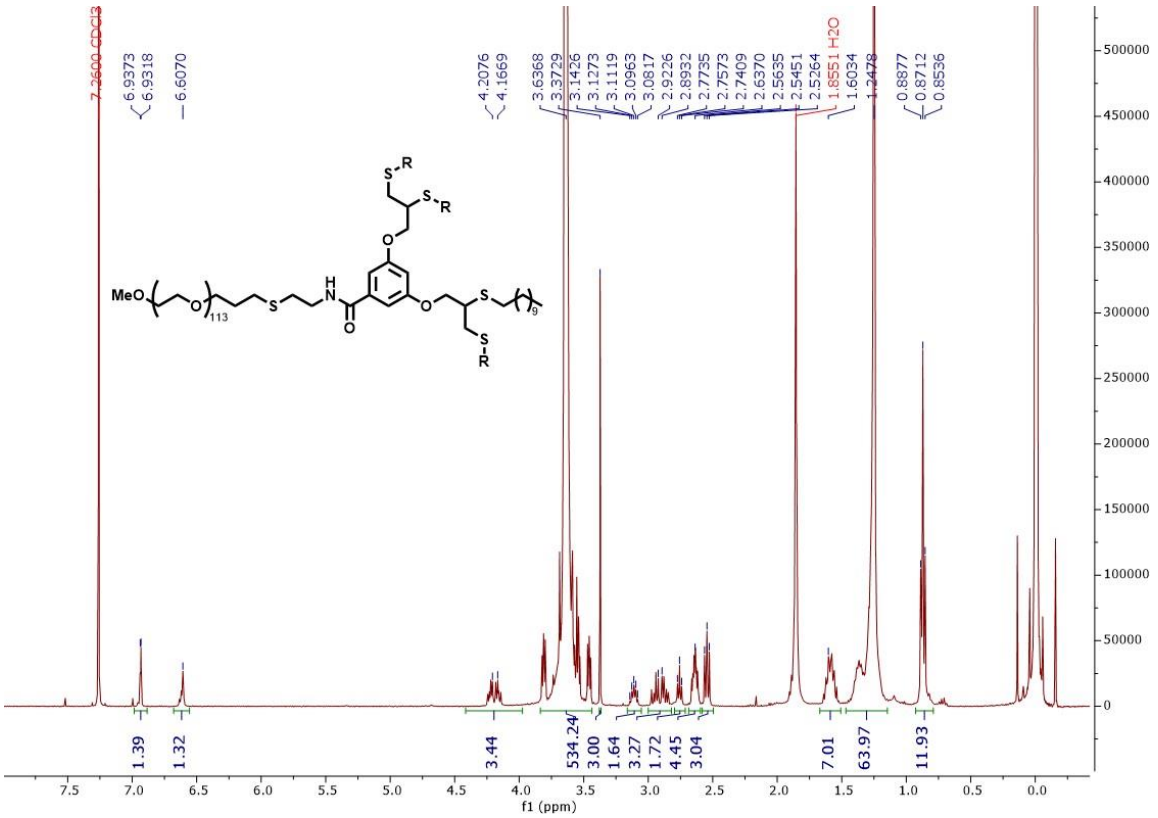

Figure S5: ^{1}H-NMR spectrum of mPEG$_{5k}$-D-(C11)$_4$ (3,5) (***C11x4 (3,5)***) in CDCl$_3$.

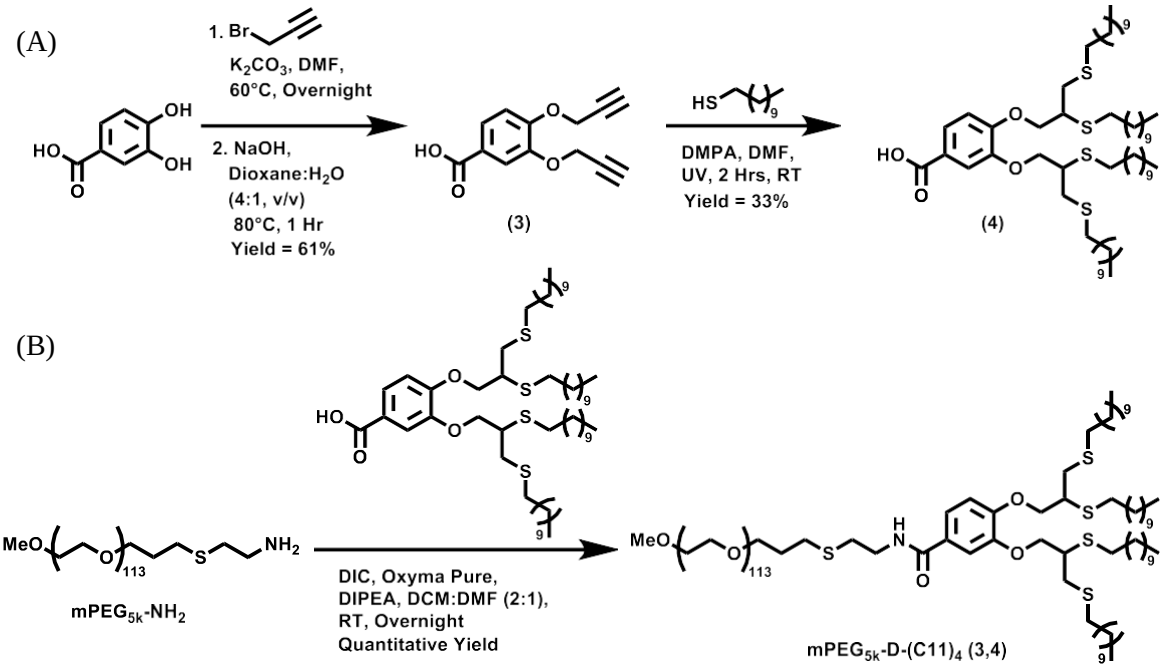

Figure S6: Synthesis of (A) C11x4 (3,4) dendron (**4**) and (B) mPEG$_{5k}$-D-(C11)$_4$ (3,4) (***C11x4(3,4)***) amphiphile**.**

3,4-bis(prop-2-yn-1-yloxy)benzoic acid was synthesized by reacting 3,4 dihydroxybenzoic acid (1.54 gr, 10 mmol) with propargyl bromide (7.2 gr, 60 mmol) and K_2CO_3 (8.3 gr, 60 mmol) in 25 mL DMF at 60°C overnight. The reaction mixture was treated with 4N NaOH in 60 mL (4:1, v/v) Dioxane:water solution. The organic solvents were evaporated, and the product was precipitated using 3N HCl to give the final product in 61% yield (1.4 gr).

^{1}H-NMR (400 MHz, DMSO-d_6): δ 7.62-7.57 (m, 2H, Ar-***H***), 7.14 (d, *J* =1.8 Hz, 1H, Ar-***H***), 7.07 (d, *J* =8.4 Hz, Ar-***H***-), 6.16-5.94 (m, 2H, Ar-O-CH_2-C***H***=CH_2), 5.55-5.15 (m, 4H, Ar-O-CH_2-CH=C***H***$_2$), 4.78-4.51 (m, 4H, Ar-O-C***H***$_2$-CH-). ^{13}C-NMR (100 MHz, DMSO-d_6): δ 167.2, 151.9, 147.4, 133.7, 133.4, 123.5, 123.2, 117.9, 117.5, 114.2, 112.8, 69.0, 68.9, 40.1, 39.9, 39.7, 39.5, 39.3, 39.1, 38.9. MS calculated for $C_{13}H_{14}O_4$ 233.08 ($(M-H)^-$), found 233.17.

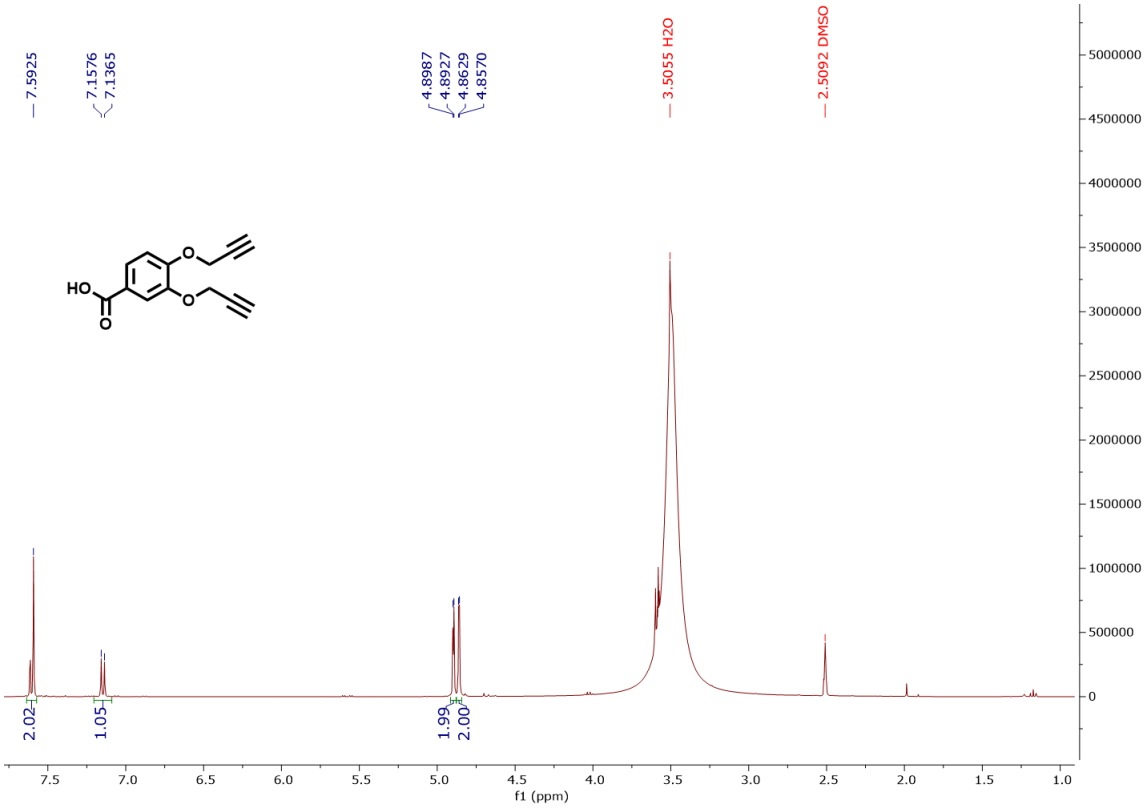

Figure S7: ^{1}H-NMR spectrum of 4,5-bis(propargyloxy)benzoic acid in DMSO-d_6.

For making the four-armed C11 amphiphile at 3,4 positions (***C11x4 (3,4)***), we made the dendritic part separately. 3,4-bis(prop-2-yn-1-yloxy)benzoic acid (50 mg, 0.218 mmol), 1-undecanethiol (1.6 gr, 1.95 mL, 8.7 mmol) and AIBN (166.2 mg, 0.872 mmol, 10 mol% with respect to the thiol) were dissolved in DMF. The solution was purged with nitrogen for 20 minutes and then stirred at 80°C

overnight. The product was purified using silica column chromatography using DCM:ethyl acetate solvent mixture (100:0 to 95:5 gradient) and was obtained in 34% yield (73 mg).

^{1}H-NMR (400 MHz, $CDCl_3$): δ 7.76 (dd, *J*=1.9 Hz, 8.4 Hz, 1H Ar-***H***), 7.63 (d, *J*=2.0 Hz, 1H, Ar-***H***), 3.28-2.84 (m, 6H, -C***H***-S- + -CH-C***H***$_2$-S-), 2.74-2.49 (m, 8H, -CH$_2$-C***H***$_2$-S-), 1.70-1.49 (m, 8H, -C***H***$_2$-CH$_2$-S-), 1.48-.1.12 (m, 64 H, -CH$_2$-C***H***$_2$-C***H***$_2$-CH$_2$- + -C***H***$_2$-CH$_3$), 0.96-0.80 (m, 12H, -CH$_2$-C***H***$_3$) ^{13}C-NMR (100 MHz, $CDCl_3$): δ 171.0, 153.4, 148.2, 125.1, 122.2, 115.1, 112.5, 70.9, 70.6, 45.3, 35.0, 33.6, 32.2, 32.1, 30.1, 29.9, 29.8, 29.7, 29.5, 29.4, 29.1, 22.8, 14.2. MS calculated for $C_{57}H_{106}O_4S_4$ 1005.69 ((M+Na)$^+$), found 1005.97.

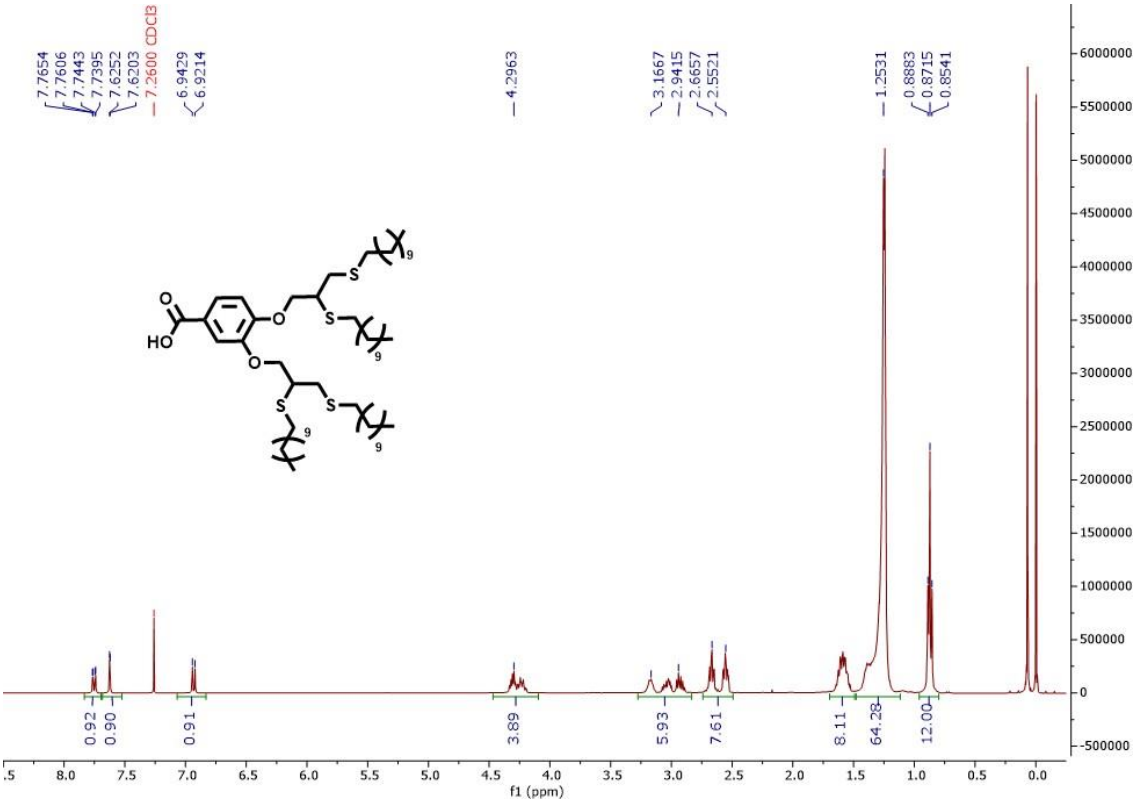

Figure S8: ^{1}H-NMR of four-armed C11(3,4) dendron in $CDCl_3$.

Then, the four-armed C11(3,4) dendron (68 mg, 0.068 mmol) was coupled to mPEG$_{5k}$-NH$_2$ (70 mg, 0.0137 mmol) using DIC (9 mg, 11 µL, 0.068 mmol), Oxyma Pure (10 mg, 0.068 mmol) and DIPEA (18 mg, 24 µL, 0.137 mmol) in 1 mL of DCM by stirring the reaction mixture at room temperature overnight. The reaction mixture was loaded as-is on a MeOH-based LH20 (Sephadex®) size exclusion column. Fractions that contained the product (identified by UV light and/or coloring with iodine) were combined, the organic solvents were evaporated to dryness and the white solid was dried under high vacuum. The product was obtained in 91% yield (75 mg).

^{1}H-NMR (400 MHz, Chloroform-d): δ 7.43 (d, *J*=2.0 Hz, Ar-***H***), 7.32 (dd, *J*=2.0 Hz, 8.4 Hz 1H, Ar-***H***), 6.90 (d, *J*=8.4 Hz, 1H, Ar-***H***), 6.62 (t, *J*=5.4 Hz, 1H, -N***H***-Ar), 4.36-4.12 (m, 4H, -C***H***$_2$-O-Ar-), 3.87-3.40 (m, PEG backbone), 3.37 (s, 3H, C***H***$_3$-O-PEG), 3.22-3.09 (m, 2H, -C***H***-S-), 3.08-2.84 (m, 4H, -CH-C***H***$_2$-S-), 2.76 (t, *J*=6.5 Hz, 2H, -O-CH-C***H***$_2$-S-), 2.72-2.50 (m, 8H -CH$_2$-C***H***$_2$-S-), 1.65-1.50 (m, 8H, -C***H***$_2$-CH$_2$-S-), 1.45-1.18 (m, 64H, -CH$_2$-C***H***$_2$-C***H***$_2$-CH$_2$- + -C***H***$_2$-CH$_3$), 0.87 (t, *J*=7 Hz, 12H, -CH$_2$-C***H***$_3$). ^{13}C-NMR (100 MHz, Chloroform-d): δ 171.0, 153.4, 148.2, 125.1, 122.2, 115.1, 112.5, 70.8, 70.6, 45.3, 35.0, 33.6, 32.2, 32.0, 30.1, 29.9, 29.8, 29.7, 29.5, 29.4, 29.1, 22.8, 14.2. GPC (DMF + 25 mM NH_4Ac): expected M_n= 6.1 kDa, experimental M_n = 6.6 kDa, Đ = 1.12.

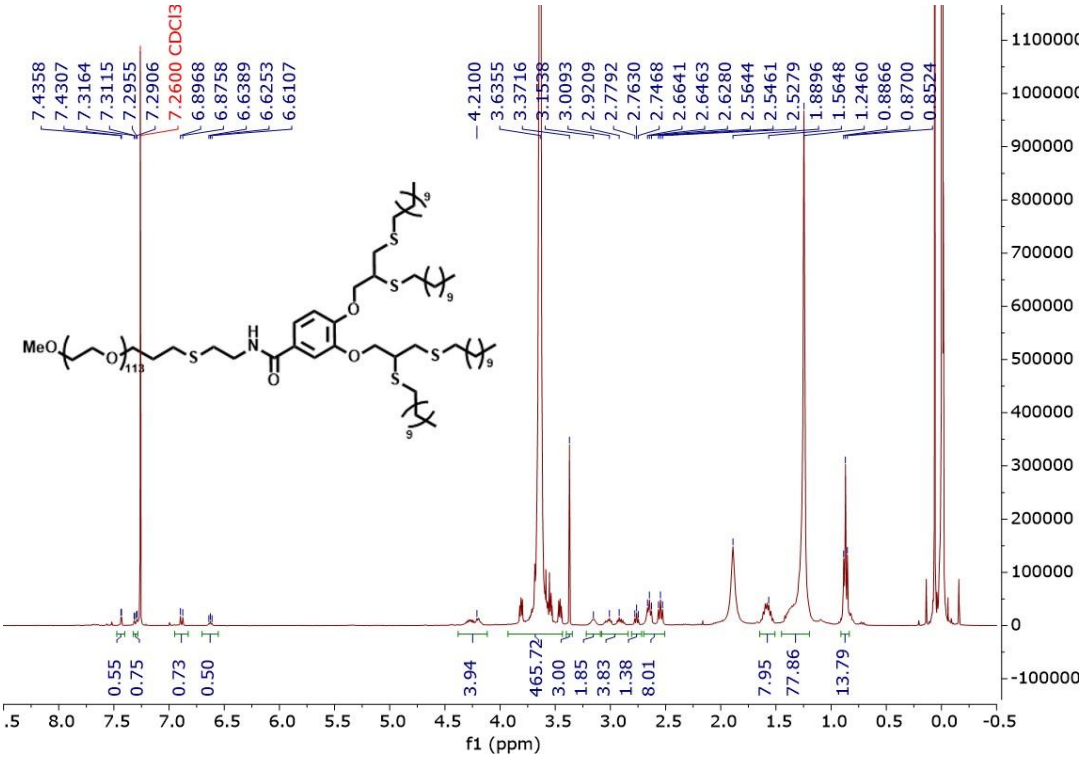

Figure S9: ^{1}H-NMR spectrum of mPEG$_{5k}$-D-(C11)$_4$ (3,4) ***C11x4(3,4)*** in $CDCl_3$.

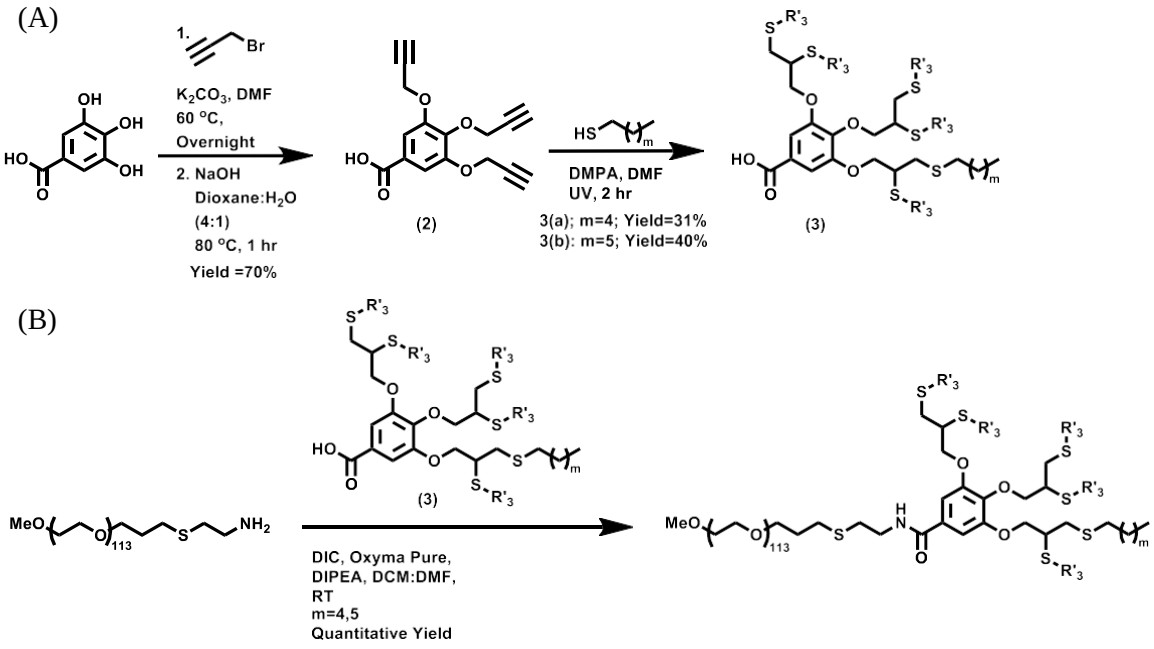

Figure S10: (A) Synthesis of six-armed dendrons and (B) six-armed amphiphiles.

3,4,5-tris(prop-2-yn-1-yloxy)benzoic acid was synthesized as previously reported.[1]

For making the six-armed amphiphiles, we synthesized the dendritic part separately by reacting 3,4,5-tris(prop-2-yn-1-yloxy)benzoic acid (100 mg, 0.352 mmol) (**2**) with either 1-hexanethiol (2.5 gr, 3 mL, 21.165 mmol) or 1-heptanethiol (2.8 gr, 3.3 mL, 21.12 mmol) and DMPA (54 mg, 0.6 eq., 0.21 mmol; 1 mol% with respect to the thiol) in 1 mL DMF. The solution was purged with nitrogen for 20 minutes and then stirred under UV light (365 nm) for 2 hours. The product was purified using silica column chromatography using hexane:ethyl acetate solvent mixture (100:0 to 85:15 gradient) to give us 31% yield (105 mg) for C6x6 dendron (**3a**) and 40% yield (149 mg) for C7x6 dendron (**3b**).

^{1}H-NMR (400 MHz, Chloroform-d): δ 7.38 (s, 2H, Ar-***H***), 4.50-4.05 (m, 6H, -C***H***$_2$-O-Ar-), 3.30-2.85 (m, 9H, -C***H***-S- + -CH-C***H***$_2$-S-), 2.80-2.42 (m, 12 H, -CH$_2$-C***H***$_2$-S-), 1.70-1.50 (m, 12 H, -C***H***$_2$-CH$_2$-S-), 1.47-.1.17 (m, 36 H, -CH$_2$-C***H***$_2$-C***H***$_2$-CH$_2$- + -C***H***$_2$-CH$_3$), 1.00-0.80 (m, 18H, -CH$_2$-C***H***$_3$) . ^{13}C-NMR (100 MHz, Chloroform-d): δ 170.3, 167.4, 164.7, 152.2, 124.2, 109.0, 70.5, 45.4, 35.1, 33.6, 32.1, 31.7, 31.6, 30.1, 30.0, 29.9, 28.7, 22.7, 14.2. MS calculated for $C_{52}H_{96}O_5S_6$ 1015.55 ($(M+Na)^+$), found 1015.92.

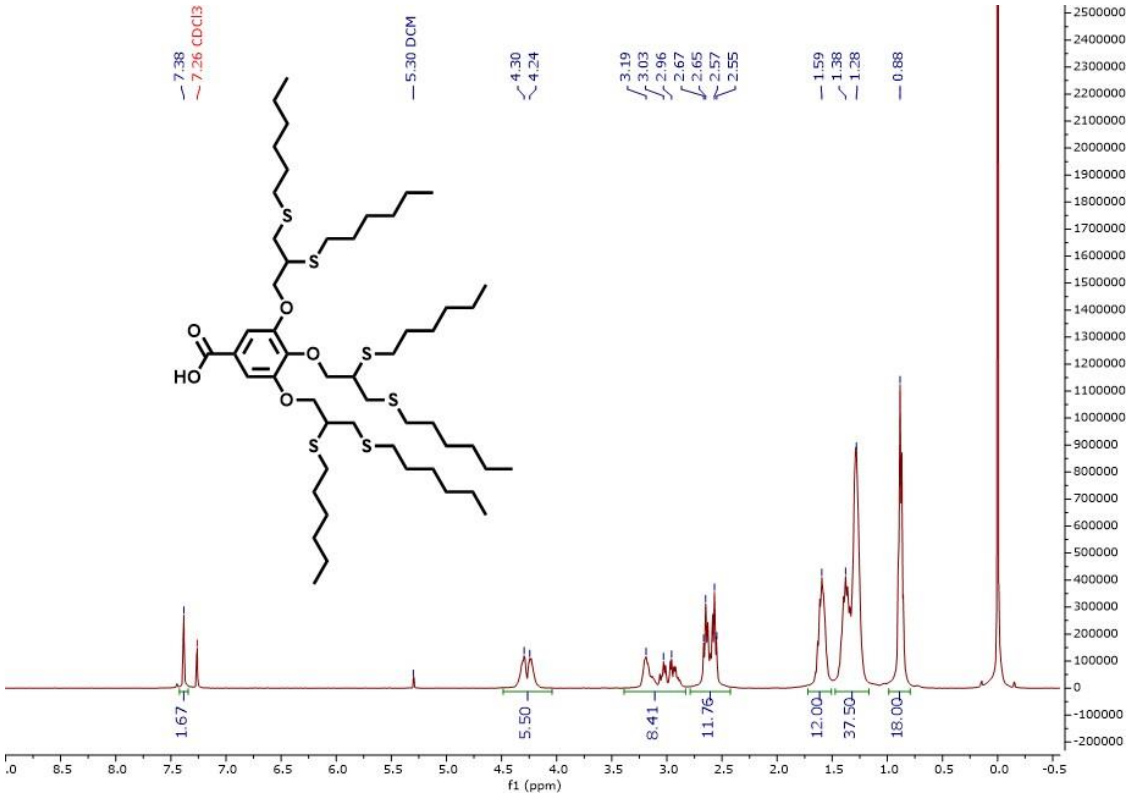

Figure S11: ^{1}H-NMR of six armed C6x6 dendron in $CDCl_3$.

^{1}H-NMR (400 MHz, Chloroform-d): δ 7.37 (s, 2H, Ar-***H***), 4.46-4.05 (m, 6H, -C***H***$_2$-O-Ar-), 3.32-2.82 (m, 9H, -C***H***-S- + -CH-C***H***$_2$-S-), 2.72-2.49 (m, 12 H, -CH$_2$-C***H***$_2$-S-), 1.69-1.50 (m, 12 H, -C***H***$_2$-CH$_2$-S-), 1.48-1.16 (m, 48H, -CH$_2$-C***H***$_2$-C***H***$_2$-CH$_2$- + -C***H***$_2$-CH$_3$), 0.96-0.80 (m, 18H, -CH$_2$-C***H***$_3$) . ^{13}C-NMR (100 MHz, Chloroform-d): δ 171.5, 152.1, 142.6, 124.3, 109.0, 74.9, 70.5, 46.5, 45.4, 35.0, 33.6, 32.1, 31.8, 30.1, 30.00, 29.9, 29.1, 29.0, 28.9, 22.7, 14.2. MS calculated for $C_{58}H_{108}O_5S_6$ 1075.66 ((M-H)$^-$), found 1076.11.

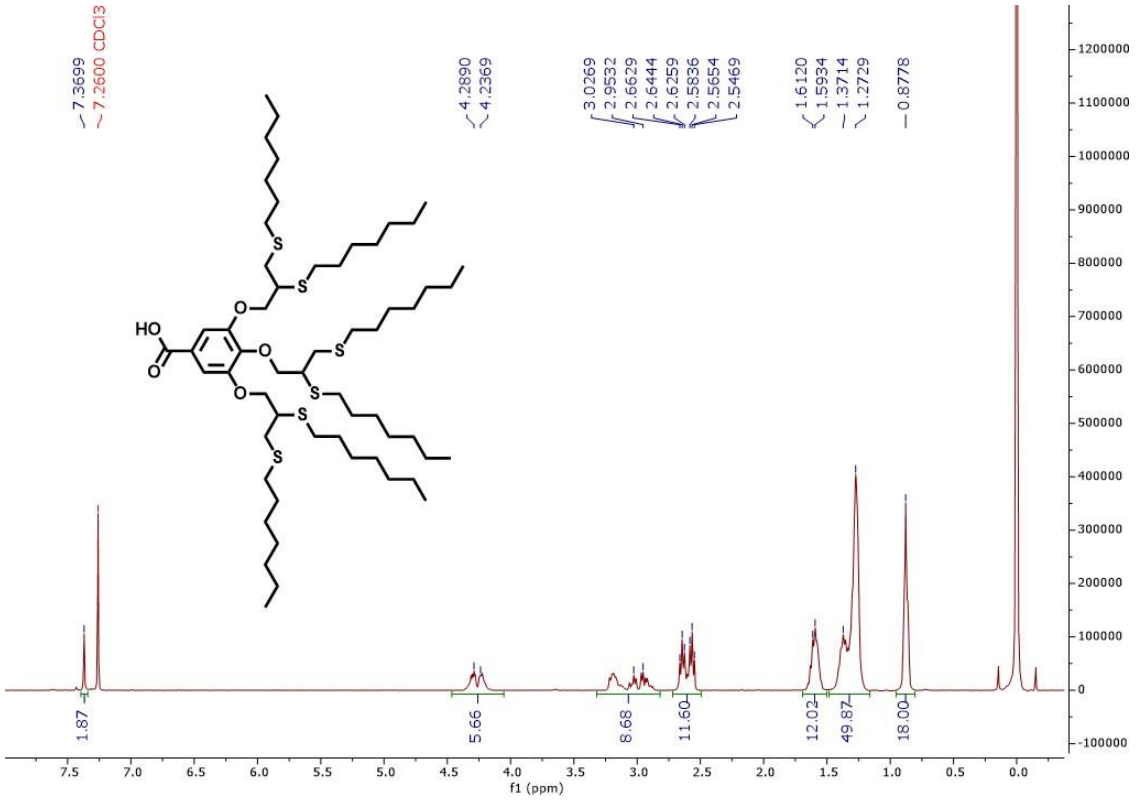

Figure S12: ^{1}H-NMR of C7x6 dendron in $CDCl_3$.

Then, the C6x6 dendron (48 mg, 0.049 mmol) was coupled to $mPEG_{5k}$-NH_2 (50 mg, 0.0097 mmol) using DIC (6 mg, 7.5 µL, 0.049 mmol) and Oxyma Pure (7 mg, 0.049 mmol) and DIPEA (6.3 mg, 8.5 µL, 0.049 mmol) in 1 mL DCM by stirring the reaction mixture at room temperature overnight. The reaction mixture was loaded as-is on a MeOH-based LH20 (Sephadex®) size exclusion column. Fractions that contained the product (identified by UV light and/or coloring with iodine) were unified, the organic solvents were evaporated to dryness and the white solid was dried under high vacuum to give the product in quantitative yield (57 mg).

^{1}H-NMR (400 MHz, Chloroform-d): δ 7.05 (s, 2H, Ar-***H***), 6.74-6.57 (t, *J*=5.6 Hz, 1H, -N***H***-Ar), 4.40-4.05 (m, 6H, C***H***$_2$-O-Ar-), 3.87-3.40 (m, PEG backbone), 3.37 (s, 3H, C***H***$_3$-O-PEG), 3.26-2.72 (m, 13H, -C***H***-S- + -CH-C***H***$_2$-S- + -CH_2-C***H***$_2$-S- + -S-C***H***$_2$-CH_2-NH-), 2.6.2.47 (m, 12H, -S-C***H***$_2$-CH_2-), 1.67-1.49 (m, 12 H, -S-CH_2-C***H***$_2$-), 1.42-1.21 (m, 36 H, -CH_2-C***H***$_2$-C***H***$_2$-CH_2- + -C***H***$_2$-CH_3), 0.94-0.81 (m, 18H, -CH_2-C***H***$_3$). ^{13}C-NMR (100 MHz, Chloroform-d): δ 166.9, 152.3, 140.5, 129.9, 106.08, 70.6, 59.1, 46.5, 45.4, 39.2, 35.0, 33.5, 32.0, 31.8, 30.0, 29.9, 29.8, 29.1, 29.0, 28.9, 28.3, 22.7, 14.2. GPC (DMF + 25 mM NH_4Ac): expected M_n= 6.1 kDa, experimental M_n = 6.0 kDa, Đ = 1.04.

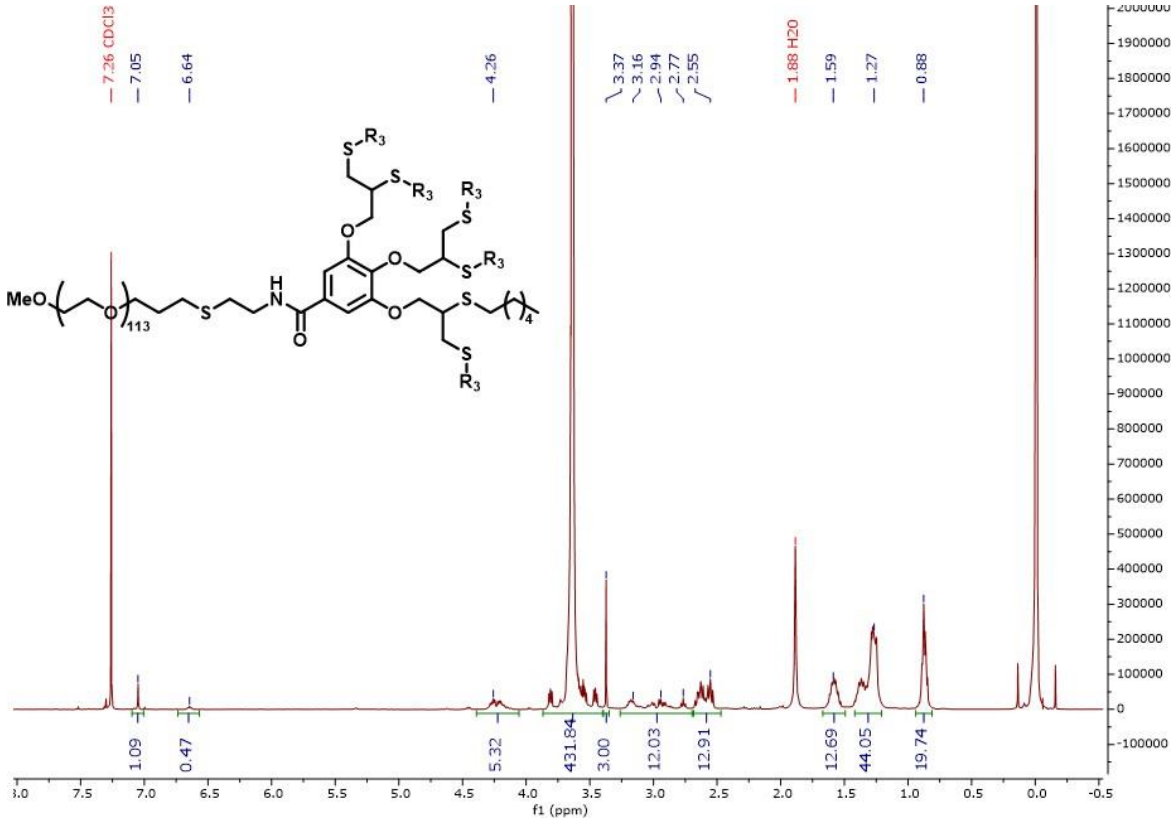

Figure S13: H-NMR spectrum of $mPEG_{5k}$-D-$(C6)_6$ (***C6x6***) in $CDCl_3$.

The C7x6 amphiphile was synthesized by coupling C7x6 dendron (48 mg, 0.049 mmol) to $mPEG_{5k}$-NH_2 (60 mg, 0.0117 mmol) using DIC (7.4 mg, 9 µL, 0.059 mmol) and Oxyma Pure (8.4 mg, 0.059 mmol) and DIPEA (15 mg, 20.4 µL, 0.117 mmol) in 1 mL DCM by stirring the reaction mixture at room temperature overnight. The reaction mixture was loaded as-is on a MeOH-based LH20 (Sephadex®) size exclusion column. Fractions that contained the product (identified by UV light and/or coloring with iodine) were unified, the organic solvents were evaporated to dryness and the white solid was dried under high vacuum to give the product in 76% yield (55 mg).

^{1}H-NMR (400 MHz, Chloroform-d): δ 7.04 (s, 2H, Ar-***H***), 6.64 (t, *J* =5.5 Hz, 1H, -N***H***-Ar), 4.49-3.99 (m, 6H, C***H***$_2$-O-Ar-), 3.87-3.40 (m, PEG backbone), 3.37 (s, 3H, C***H***$_3$-O-PEG), 3.27-2.47 (m, 25H, -C***H***-S- + -CH-C***H***$_2$-S- + -CH$_2$-C***H***$_2$-S- + -S-C***H***$_2$-CH$_2$-NH- + -S-C***H***$_2$-CH$_2$-), 1.87 (quin, *J* = 6.6 Hz, 2H, -O-CH$_2$-C***H***$_2$-CH$_2$-S-), 1.71-1.44 (m, 12H, -S-CH$_2$-C***H***$_2$-), 1.42-1.18 (m, 48H, -CH$_2$-C***H***$_2$-C***H***$_2$-CH$_2$- + -C***H***$_2$-CH$_3$), 0.97-0.76 (m, 18H, -CH$_2$-C***H***$_3$). ^{13}C-NMR (100 MHz, Chloroform-d) δ 166.9, 152.3, 140.5, 129.9, 108.5, 106.1, 77.5, 77.1, 76.8, 70.6, 59.1, 46.5, 46.4, 45.4, 39.2,

35.0, 33.5, 32.0, 31.8, 30.0, 29.96, 29.8, 29.1, 29.0, 28.9, 28.3, 22.7, 14.2. GPC (DMF + 25 mM NH_4Ac): expected M_n= 6.2 kDa, experimental M_n = 5.7 kDa, Đ = 1.07.

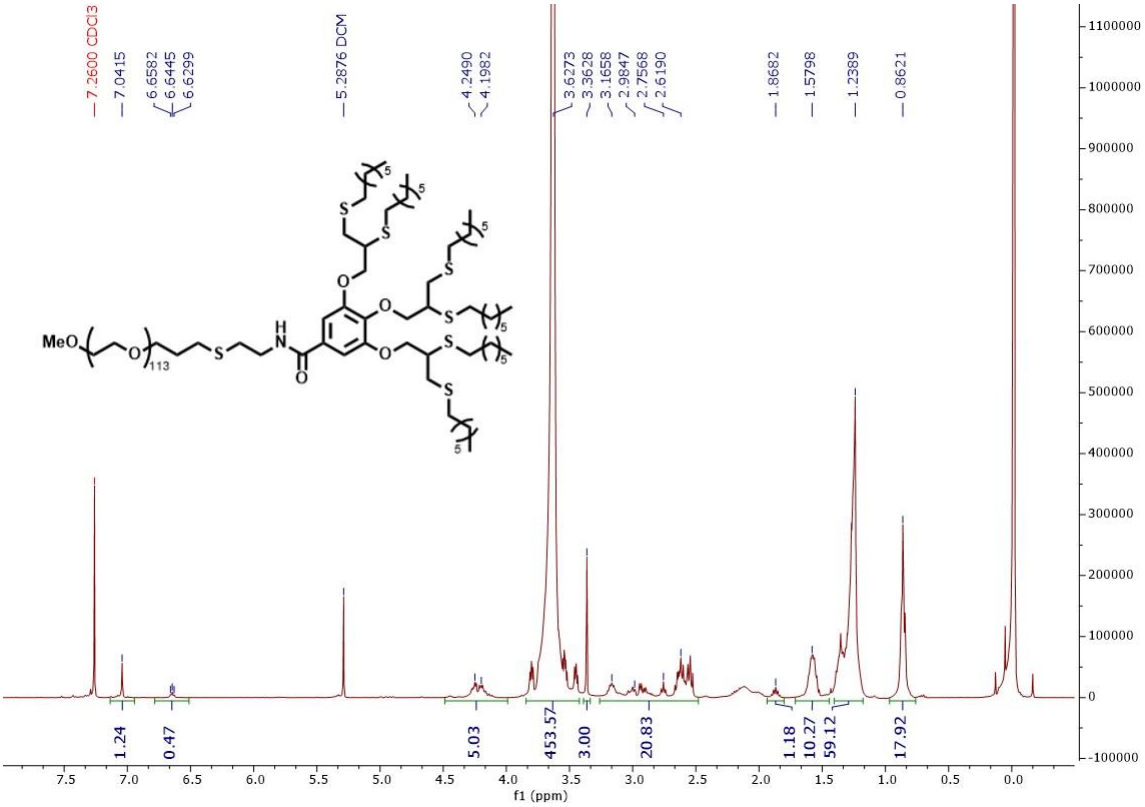

Figure S14: ^{1}H-NMR spectrum of $mPEG_{5k}$-D-$(C7)_6$ (***C7x6***) in $CDCl_3$.

2.1 Synthesis of propargylated substrates

para-Nitrophenol propargyl ether (PNPPE) and N-para-nitrophenyl O-propargyl carbamate (PNACAPE) were synthesized as previously reported[2,3] and the spectroscopic characterization correlated well with these reports.

^{1}H-NMR (400 MHz, Chloroform-d): δ 8.23 (d, *J* =9.3 Hz, 2H, Ar-***H***), 7.06 (d, *J* =9.3 Hz, 2H, Ar-***H***), 4.80 (d, *J* =2.4 Hz, 2H, -O-C***H***$_2$-C≡CH), 2.59 (t, *J* =2.5 Hz, 1H, -C≡C***H***). ^{13}C-NMR (100 MHz, Chloroform-d): δ 162.4, 142.2, 125.9, 115.1, 77.2, 76.8, 56.4.

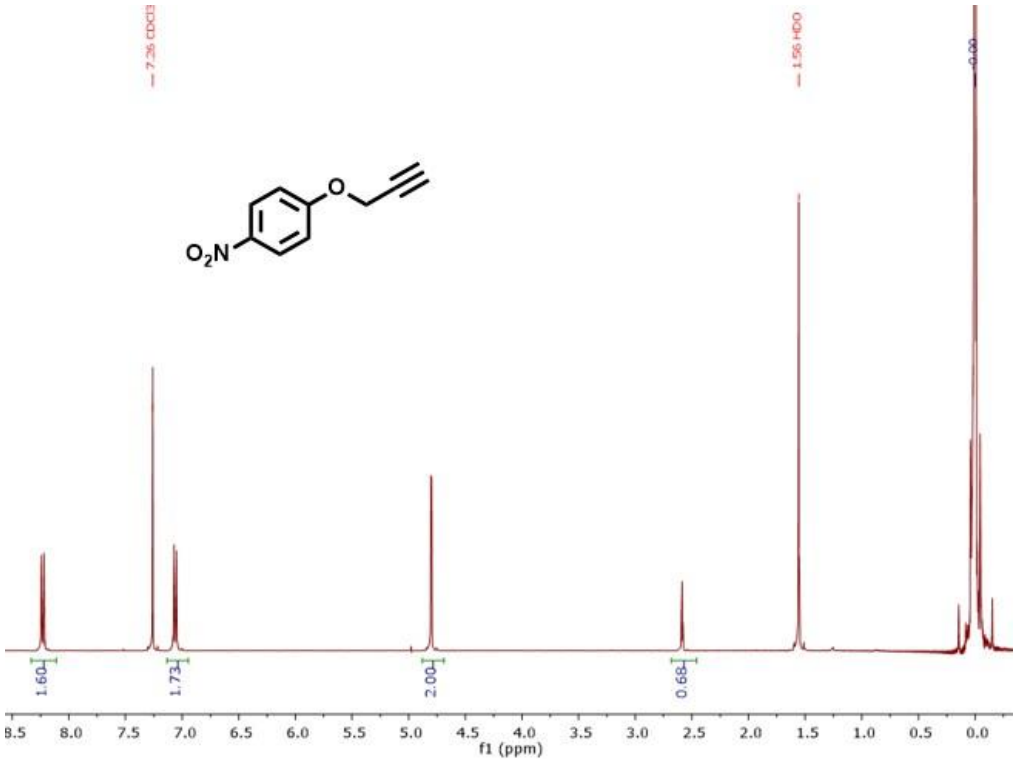

Figure S15: ^{1}H-NMR spectrum of para-nitrophenol propargyl ether in $CDCl_3$.

^{1}H-NMR (400 MHz, DMSO-d6) δ 10.58 (s, 1H, Ar-N***H***-COO-), 8.22 (d, *J* =9.3 Hz, 2H, Ar-***H***), 7.69 (d, *J* =9.3 Hz, 2H, Ar-***H***), 4.82 (d, *J* =2.4 Hz, 2H, -O-C***H***$_2$-C≡CH), 3.61 (t, *J* =2.4 Hz, 1H, -C≡C***H***). ^{13}C-NMR (100 MHz, DMSO) δ 153.3, 146.2, 142.8, 126.0, 118.7, 79.4, 78.9, 53.5, 40.4.

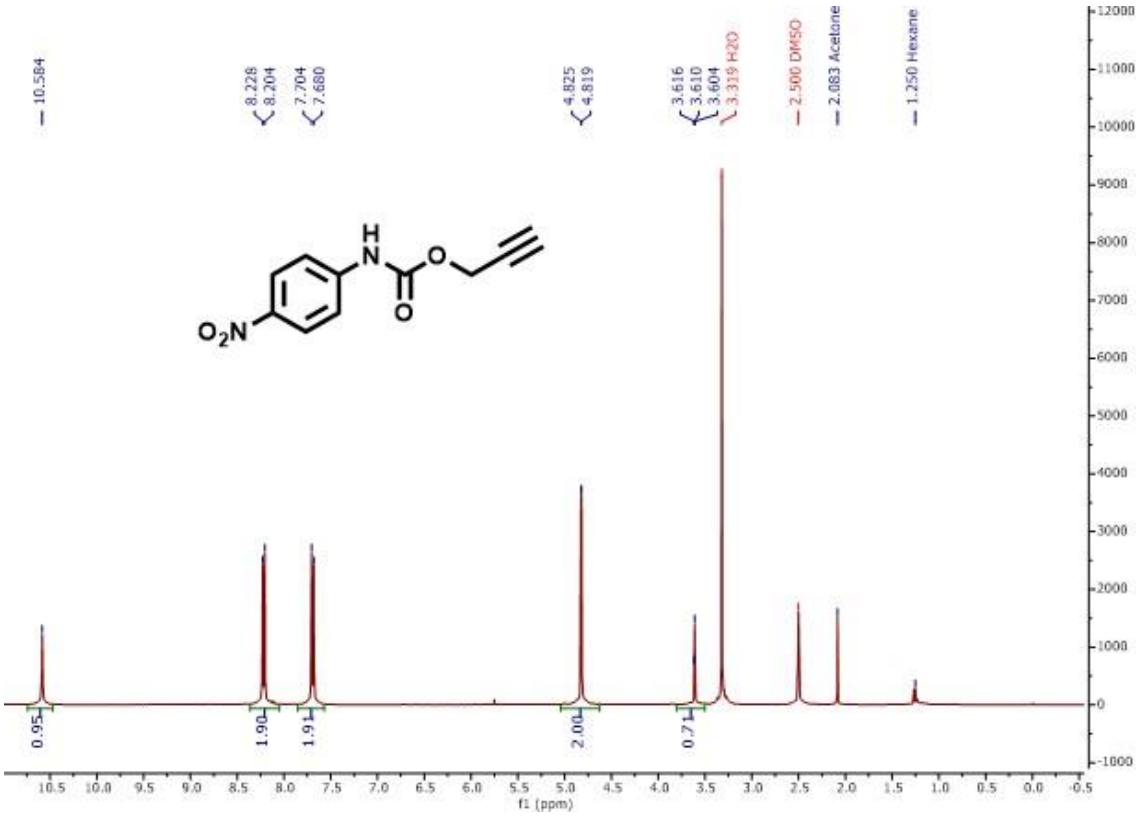

Figure S16: ^{1}H-NMR spectrum of N-para-nitrophenyl O-propargyl carbamate in $CDCl_3$.

3. Characterization of PEG-dendron hybrids

3.1. HPLC measurements

Instrument: Waters Alliance e2695

Column: Aeris WIDEPORE, C4, 3.6 µm, 150x4.6 mm

Column temperature: 30°C

Sample temperature: 37°C

Solution A: 0.1% $HClO_4$:ACN 95:5 v/v

Solution B: 0.1% $HClO_4$:ACN 5:95 v/v

Solution C: ACN

Flow rate: 1 mL/min

Gradient program for 15 minutes injection:

Time (minutes)	Solution A (%)	Solution B (%)	Solution C (%)
0	0	95	5
1	50	45	5
8	95	0	5
10	95	0	5
10.1	0	95	5
15	0	95	5

Injection volume: 30 µL

Seal wash: H_2O:MeOH 90:10 v/v

Needle wash: MeOH

Detector: Waters 2998 photodiode array detector

Sampling rate: 2 points/GPC

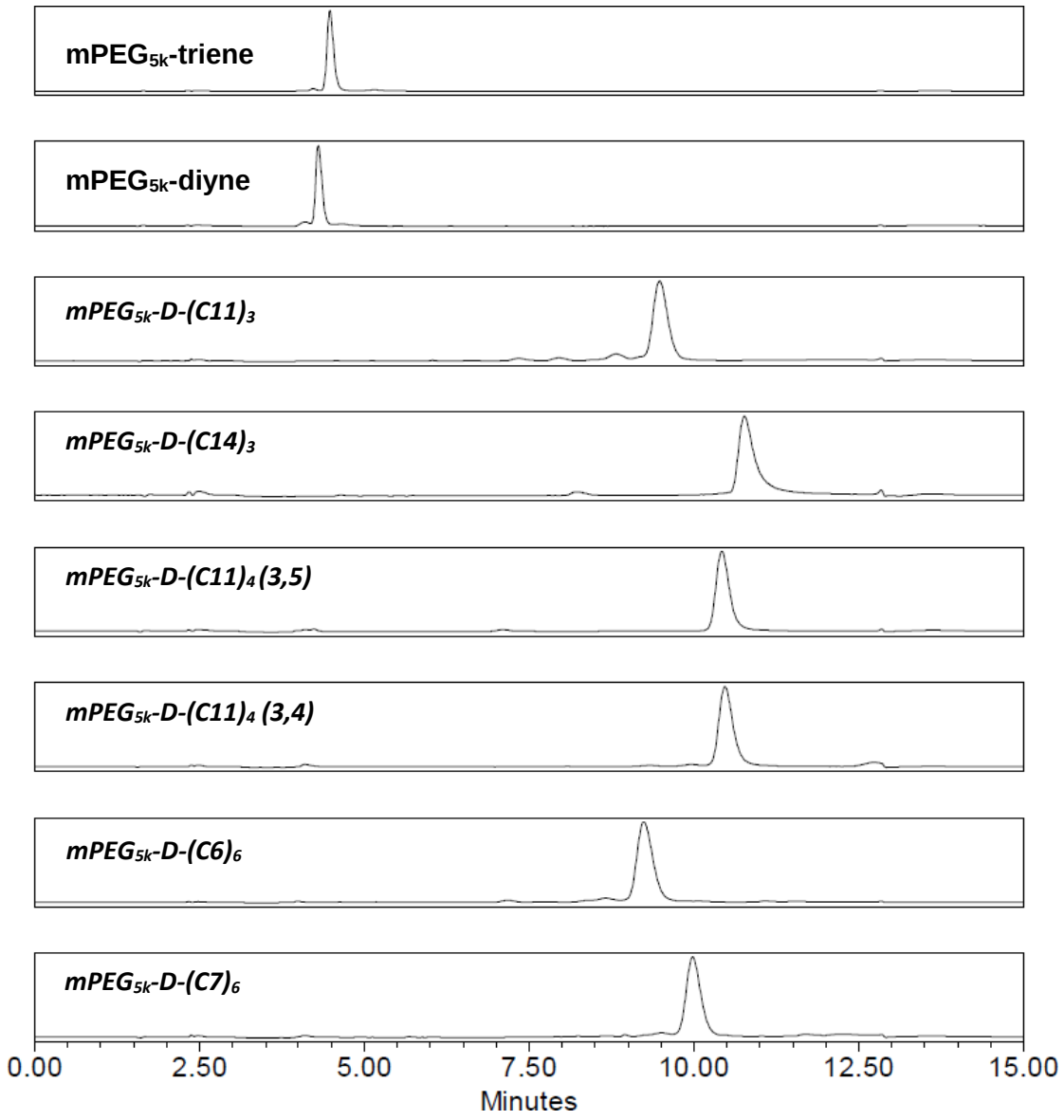

Figure S17: HPLC chromatogram overlay of hybrids.

3.2 Gel Permeation chromatography (GPC)

Instrument method:

Instrument: Malvern Viscotek GPCmax

Columns: 2xPSS GRAM 1000Å

Column temperature: 50°C

Flow rate: 0.5 mL/min

Injection time: 60 min

Injection volume: 50 µL from a 10 mg/mL sample

Diluent + mobile phase: DMF+ 25 mM NH_4Ac

Needle wash: DMF

Detector: Viscotek VE3580 RI detector

Sample preparation: The amphiphiles were directly dissolved in the diluent to give a final concentration of 10 mg/mL and filtered with 0.45 µm PTFE syringe filter.

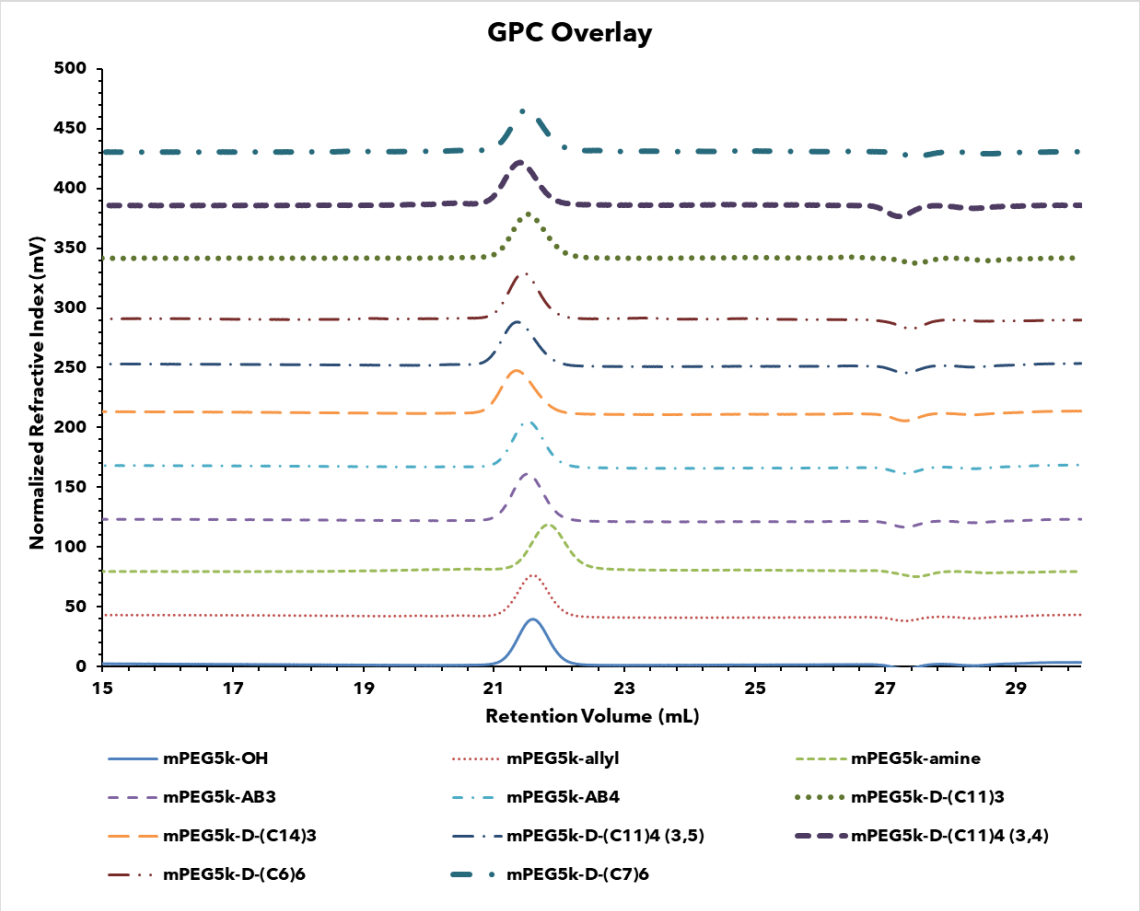

Figure S18: GPC traces overlay of synthesized polymers and final amphiphiles.

3.3 Critical micelles' concentration (CMC)

General procedure of measurement:

Preparation of diluent:

Nile Red stock solution (0.88 mg/mL in ethanol) was diluted into a phosphate buffer saline (137 mM NaCl, 10 mM phosphate, 2.7 mM KCl; pH 7.4) to afford a final concentration of 1.25 µM.

Preparation and measurement of samples:

The PEG-dendron amphiphiles were directly dissolved in the diluent to give a final concentration of 500 µM. Solution was vortexed vigorously until the amphiphile completely dissolved and further sonicated for 15 minutes in an ultrasonic bath. The solutions were consecutively diluted by a factor of 1.5 with the diluent to afford a series of 24 samples for each amphiphile. 150 µL of each sample was loaded onto a 96 well plate and a fluorescence emission scan was performed for each well. To determine the hybrid's CMC– the maximum emission of Nile Red (at about 630 nm) was plotted as a function of the amphiphile's concentration. This procedure was repeated thrice for each amphiphile, and mean value is reported as the CMC value and the standard deviation as measurement error.

Instrument method: Instrument: TECAN InfiniteM200Pro

Excitation: 550 nm

Emission intensity scan: 580-800 nm

Step: 2 nm

Number of flashes: 5

Gain: 100

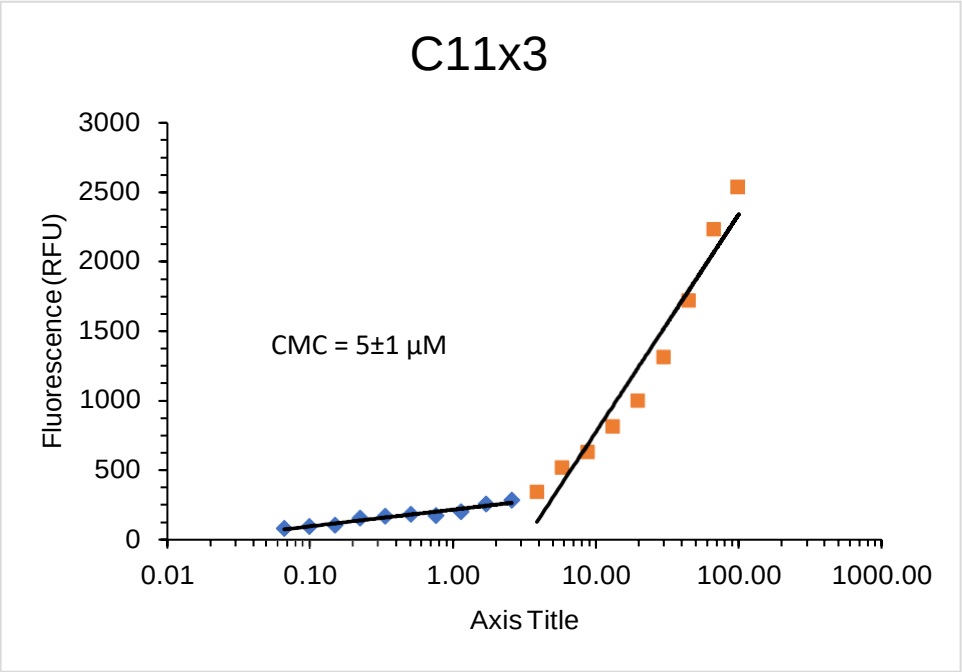

Figure S19: CMC measurement of C11x3 amphiphile ($mPEG_{5k}$-D-$(C11)_3$).

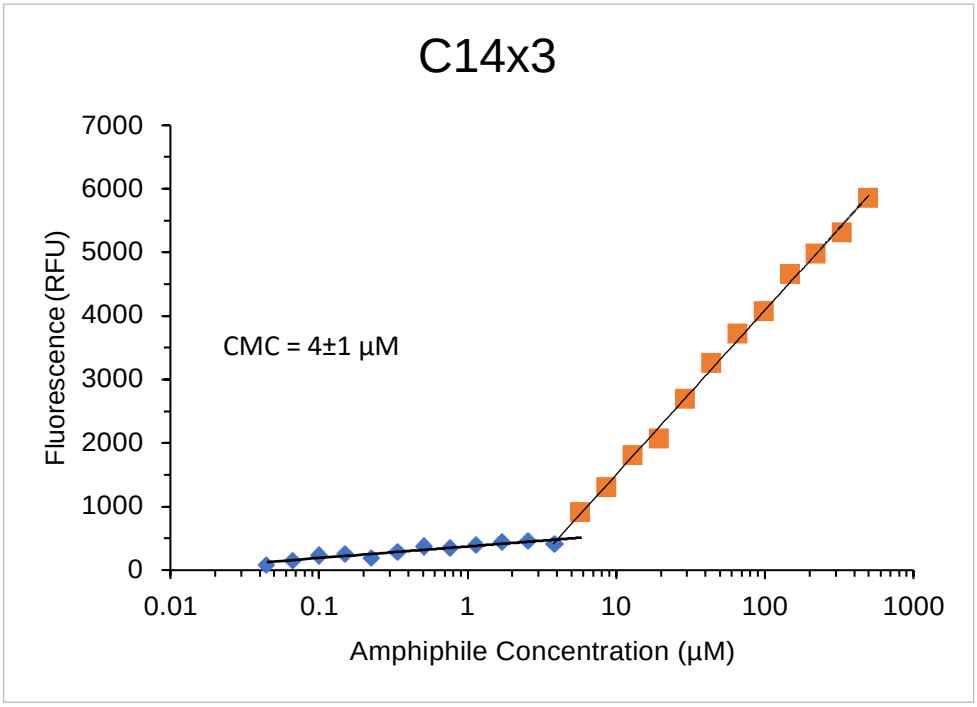

Figure S20: CMC measurement of C14x3 amphiphile ($mPEG_{5k}$-D-$(C14)_3$).

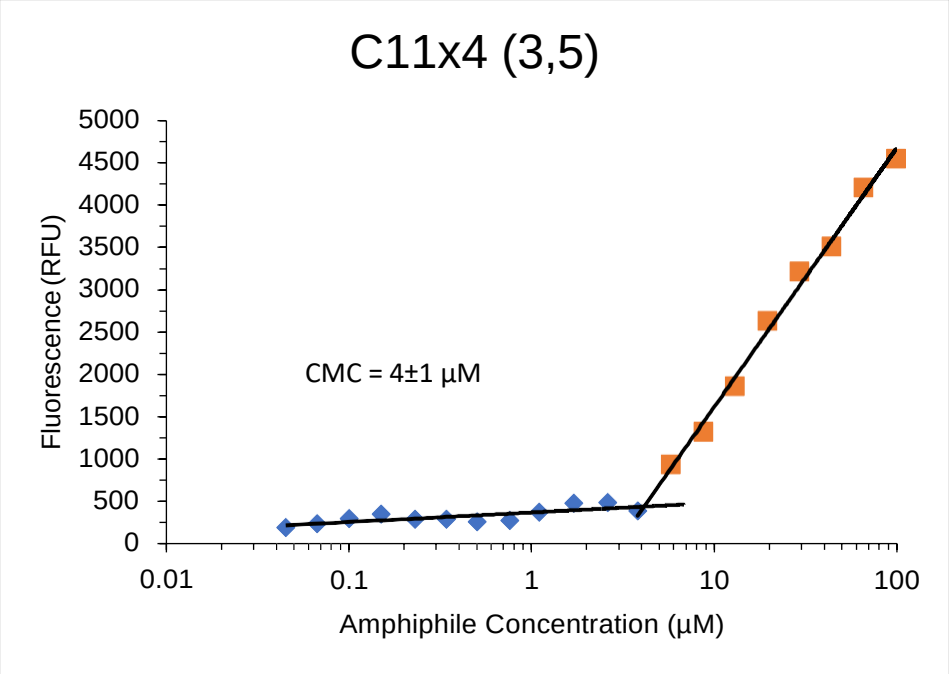

Figure S21: CMC measurement of C11x4 (3,5) amphiphile ($mPEG_{5k}$-D-$(C11)_4$) (3,5).

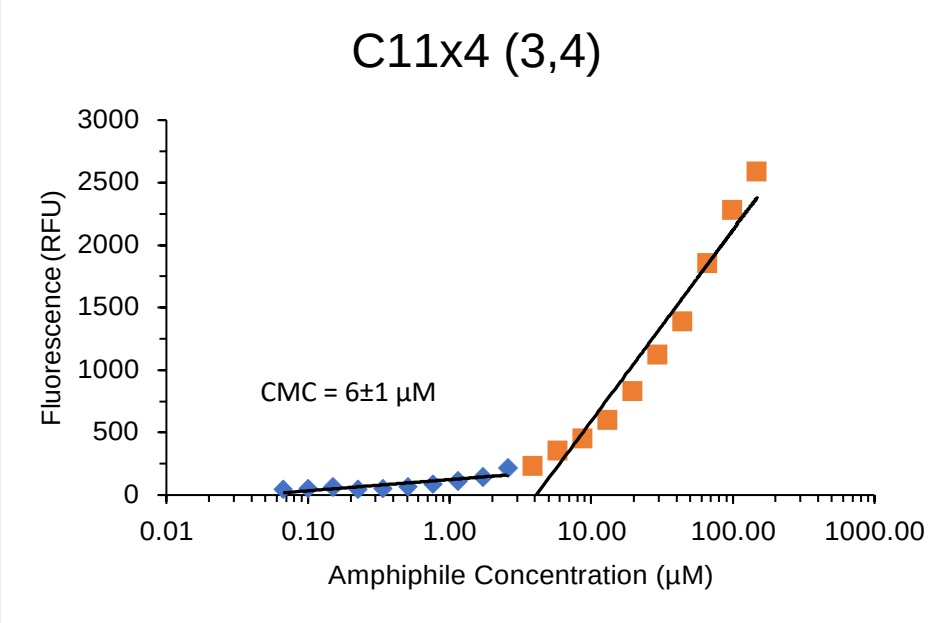

Figure S22: CMC measurement of C11x4 (3,4) amphiphile ($mPEG_{5k}$-D-$(C11)_4$) (3,4).

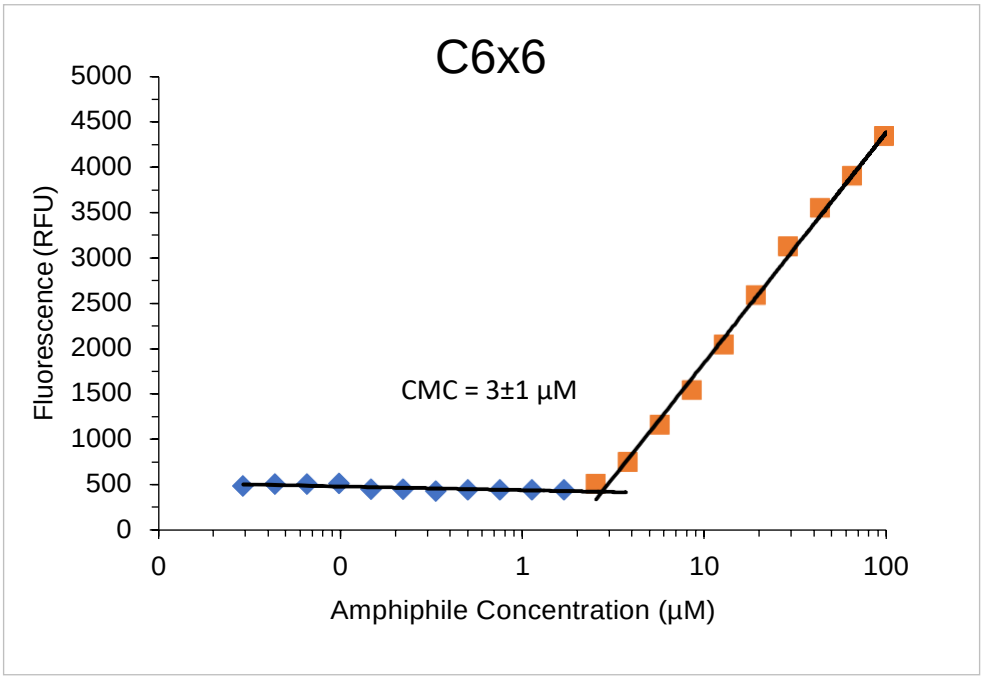

Figure S23: CMC measurement of C6x6 amphiphile ($mPEG_{5k}$-D-$(C6)_6$).

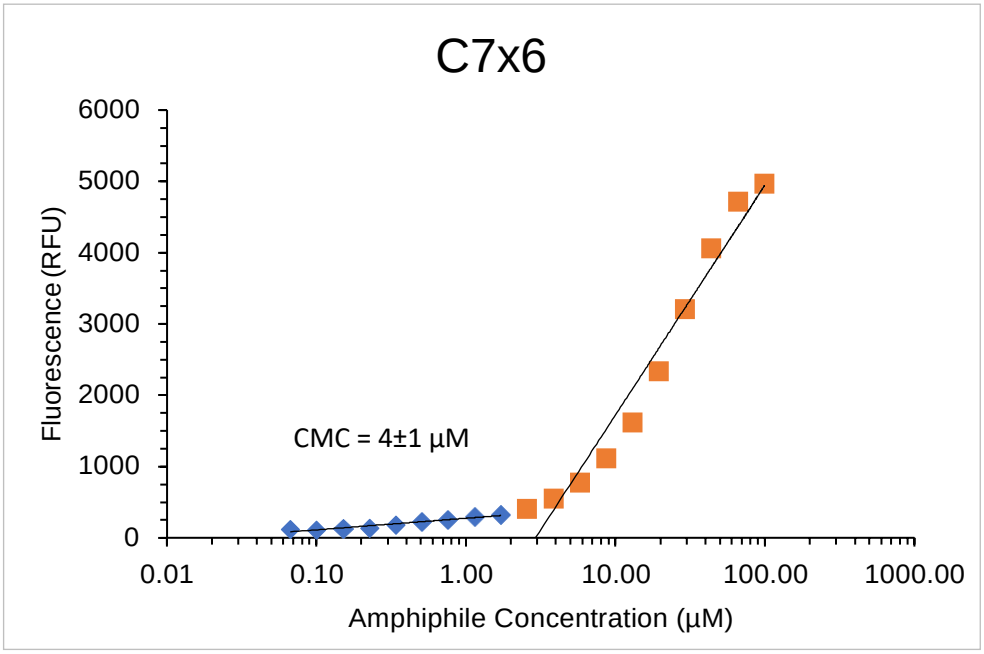

Figure S24:CMC measurement of C7x6 amphiphile ($mPEG_{5k}$-D-$(C7)_6$).

3.4 Dynamic light scattering (DLS)

Sample preparation:

Detailed sample preparation method is described under the section 4.1 "General protocol for the preparation of palladium-embedded micellar nanoreactors and depropargylation experiments setup" below. The amount of $Pd(OAc)_2$ solution was modified accordingly to yield the desired substrate:metal molar ratio.

Instrument: Corduan technology VASCOγ – particle size analyzer

Time interval: 10 µs

Number of channels: 100-650

DTC position: down

Laser power: 50-100%

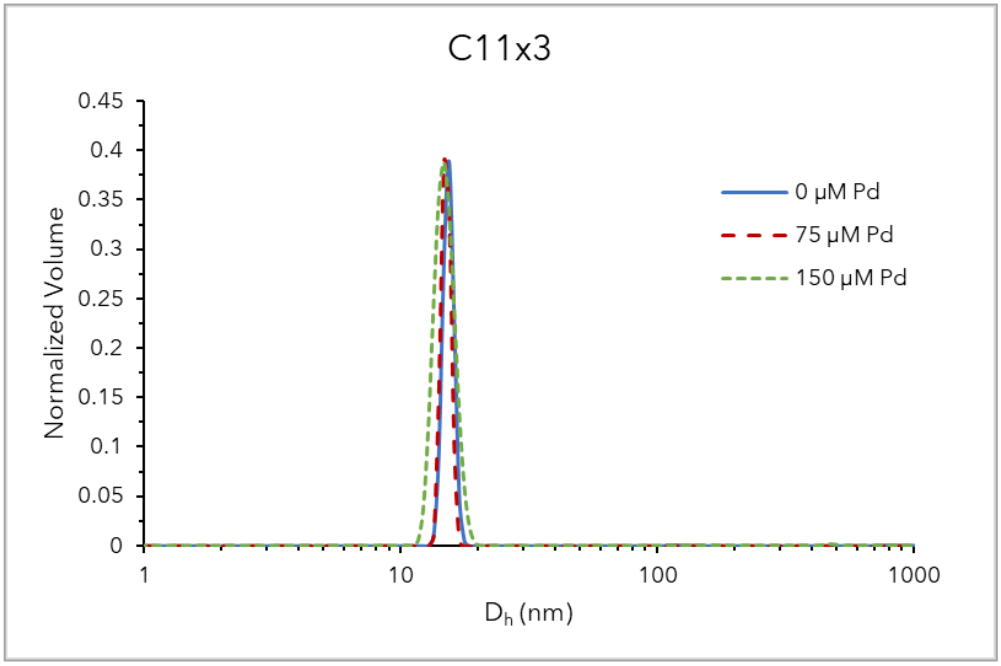

Figure S25: DLS size measurements overlay of C11x3 without $Pd(OAc)_2$ (full line; blue), with 75 µM $Pd(OAc)_2$ (large-dashed line; red) and 150 µM of $Pd(OAc)_2$ (small-dashed line; green). [Amphiphile]=320 µM.

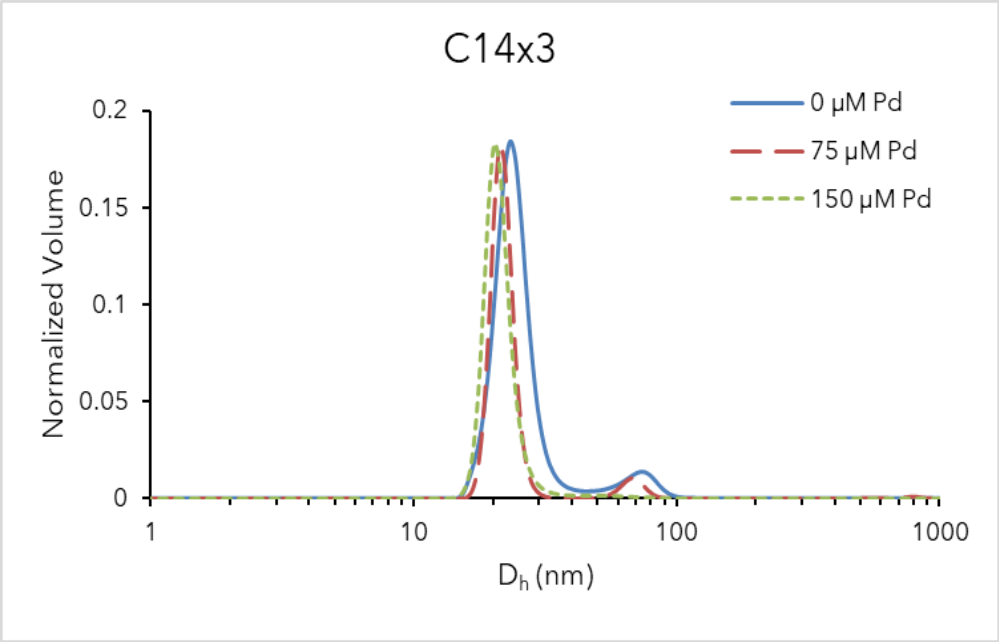

Figure S26: DLS size measurements overlay of C14x3 without $Pd(OAc)_2$ (full line; blue), with 75 µM $Pd(OAc)_2$ (large-dashed line; red) and 150 µM of $Pd(OAc)_2$ (small-dashed line; green). [Amphiphile]=320 µM.

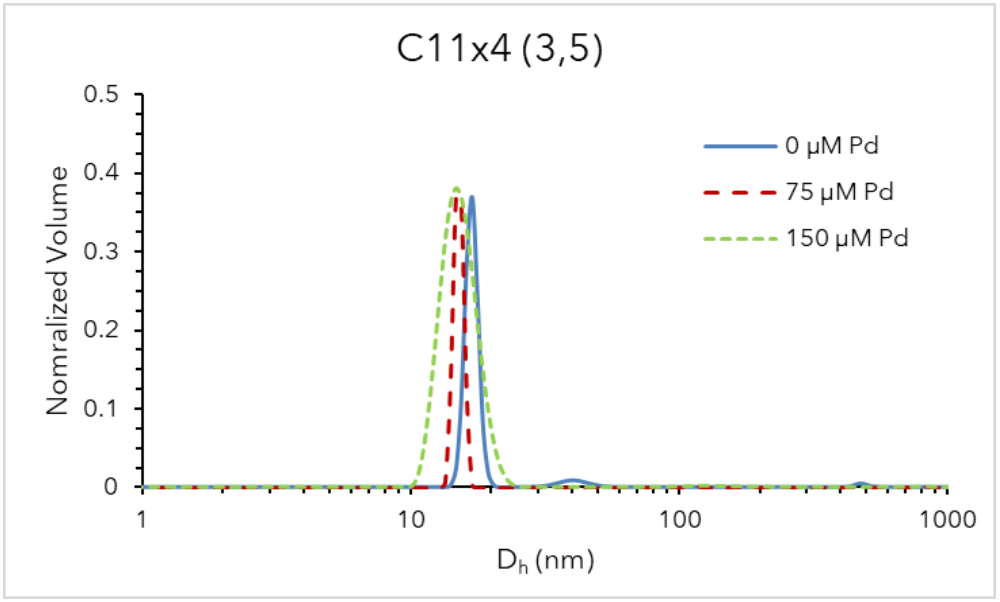

Figure S27: DLS size measurements overlay of C11x4(3,5) without $Pd(OAc)_2$ (full line; blue), with 75 µM $Pd(OAc)_2$ (large-dashed line; red) and 150 µM of $Pd(OAc)_2$ (small-dashed line; green). [Amphiphile]=320 µM.

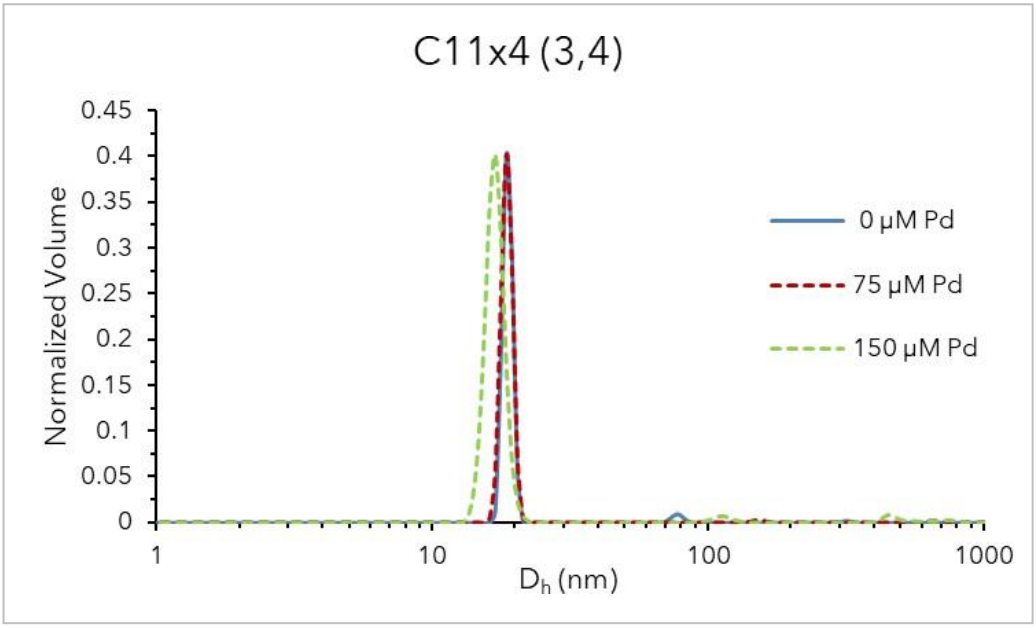

Figure S28: DLS size measurements overlay of C11x4 (3,4) without $Pd(OAc)_2$ (full line; blue), with 75 µM $Pd(OAc)_2$ (large-dashed line; red) and 150 µM of $Pd(OAc)_2$ (small-dashed line; green). [Amphiphile]=320 µM.

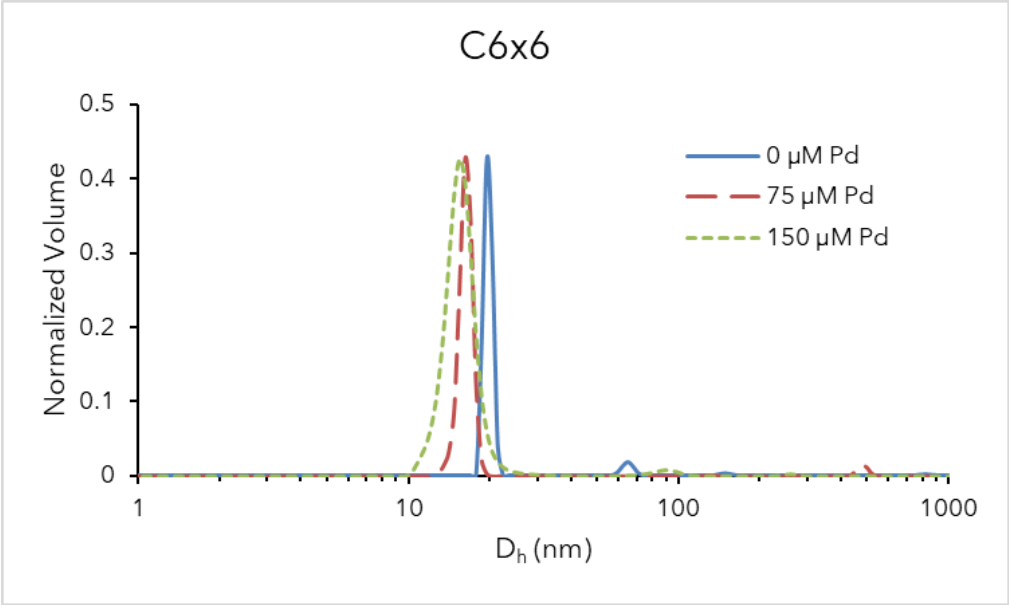

Figure S29: DLS size measurements overlay of C6x6 without $Pd(OAc)_2$ (full line; blue), with 75 µM $Pd(OAc)_2$ (large-dashed line; red) and 150 µM of $Pd(OAc)_2$ (small-dashed line; green). [Amphiphile]=320 µM.

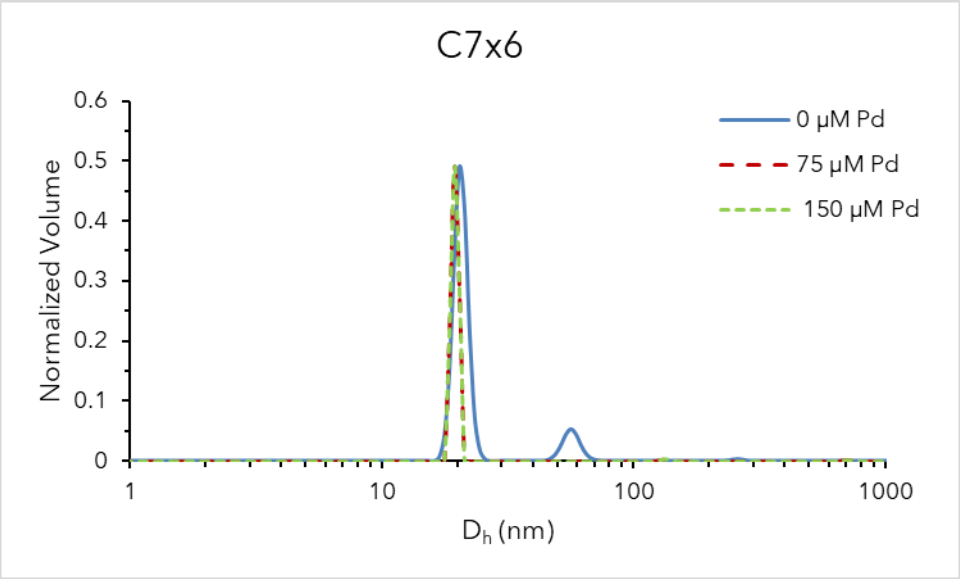

Figure S30: DLS size measurements overlay of C7x6 without $Pd(OAc)_2$ (full line; blue), with 75 µM $Pd(OAc)_2$ (large-dashed line; red) and 150 µM of $Pd(OAc)_2$ (small-dashed line; green). [Amphiphile]=320 µM.

3.5 Transmission Electron Microscopy (TEM)

Sample preparation:

The amphiphiles solution with or without Pd salt were prepared as described for the depropargylation experiments. 30 µL of the solution were dropped onto carbon coated copper grids. The excessive solvent of the droplet was wiped away using a filter paper and the sample grids were left to dry in air at RT. Then, grids were inspected in transmission electron microscope (TEM), operated at 80 kV (JEM-1400Plus).

C14X3

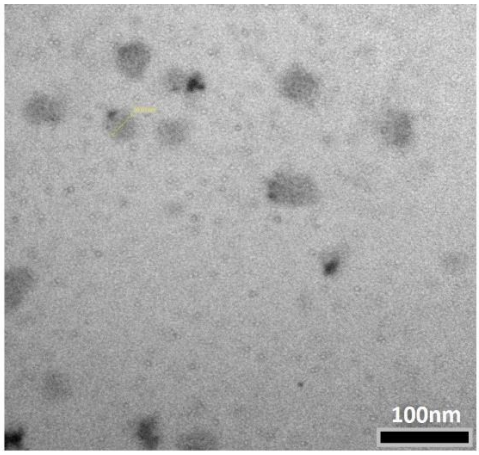

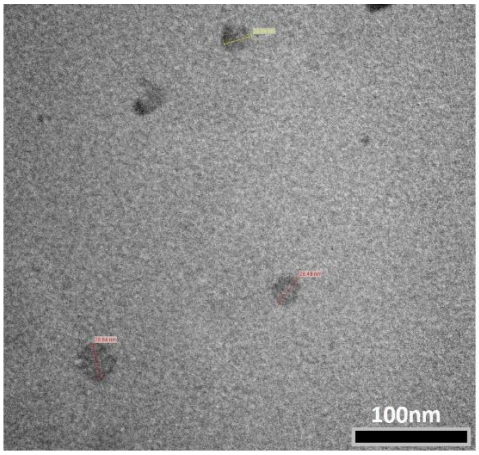

C11X3

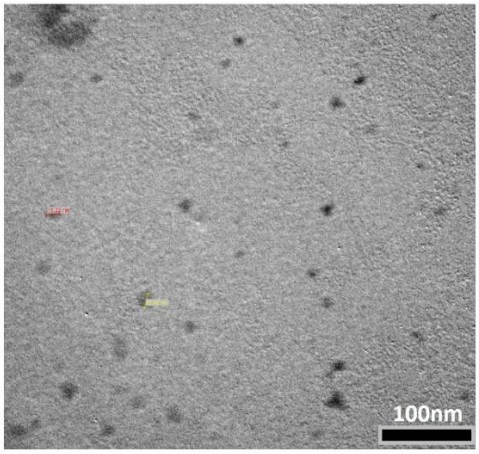

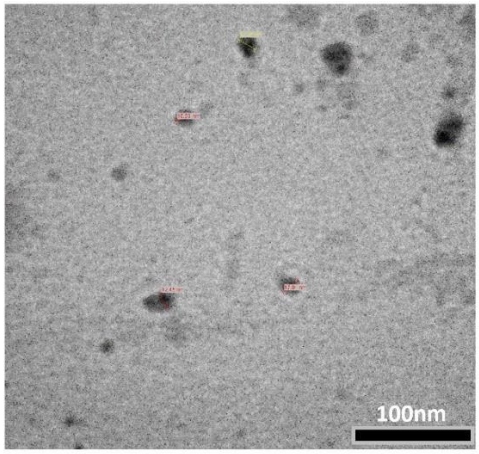

C11X4

(3,5)

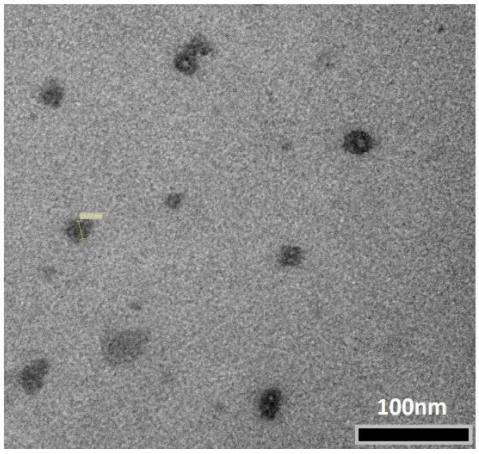

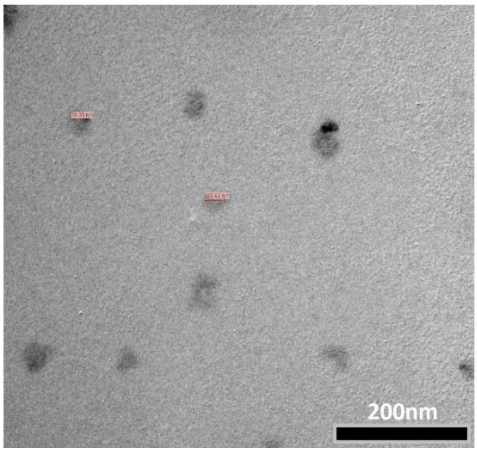

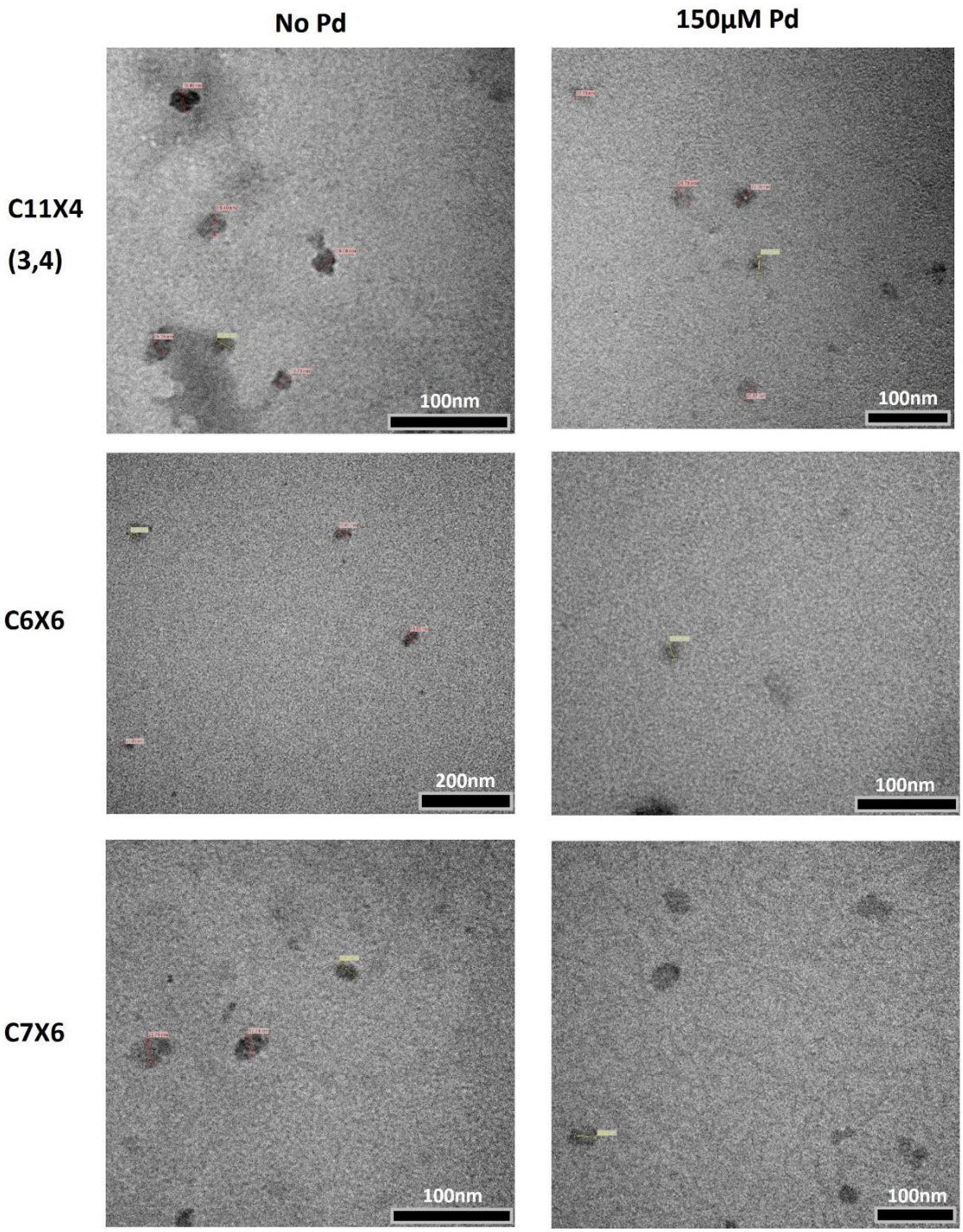

Figure S31: TEM images of the micelles based on the synthesized amphiphiles, with (right columns) and without (left columns) the presence of palladium acetate salt.

4. General Sample Preparation and Experimental Procedures

4.1 Depropargylation experiments:

General protocol for the preparation of palladium-embedded micellar nanoreactors and depropargylation experiments setup

Stock solutions of $Pd(OAc)_2$ and CX amphiphiles were made separately in acetone at a concentration of 300 µM and 640 µM, respectively. The solutions were mixed at a ratio of 1:1 v/v for solution with 150 µM $Pd(OAc)_2$ and 1:2 (Palladium stock: amphiphile stock) for solution with 75 µM stock and vortexed briefly. Acetone was removed, and the mixture was dried under high vacuum. Then, the mixture was re-dissolved in phosphate buffer saline (PBS, pH=7.4) to form the micellar nanoreactor, with final concentrations of 150 µM and 75 µM for the metal salt and 320 µM for the amphiphile, respectively. Stock solutions of the substrates were made separately by directly dissolving the solids in DMSO to give a final concentration of 40 mM for PNPPE substrate, and 20 mM for PNACAPE substrate. To initiate the reaction, the substrates were added to the aqueous nanoreactor solution (7.5 µL of substrate solution per 1 mL) and the vials were vortexed briefly. The catalysis was followed using HPLC at 37°C, by monitoring the area under the peak of the substrate at their maximum wavelength of absorbance. This procedure was repeated thrice for each set of amphiphile and substrate. Samples of amphiphiles and substrates in the absence of palladium were used as a control for monitoring the stability of the substrate solution over time and to ensure its hydrolysis cannot be catalyzed by the micellar system alone. The control of substrates and metal in the absence of the micellar structures could not be measured since the palladium salt has poor water solubility.

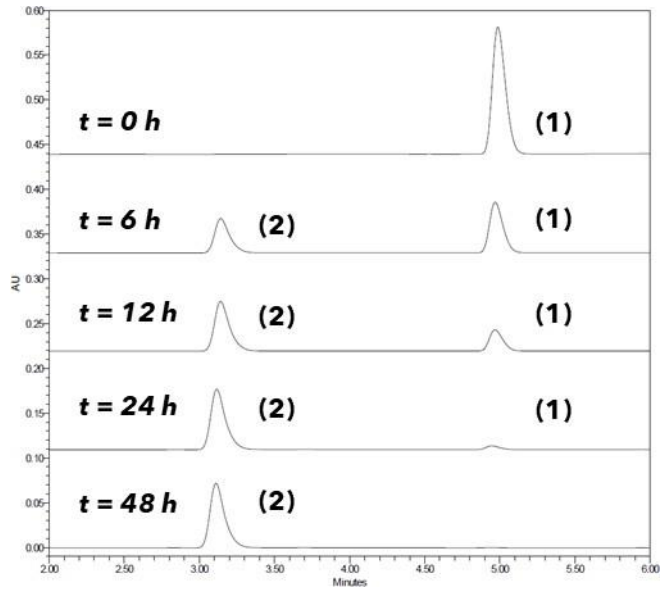

Figure S32: Representative HPLC chromatogram overlay (taken at 307 nm), showing the transformation of **PNPPE** (**1**) to paranitrophenol (**PNP**) (**2**) using palladium loaded C11x3 amphiphilic micelles ([Amphiphile] = 320 µM, [Substrate] = 300 µM, $[Pd(OAc)_2]$ = 150 µM).

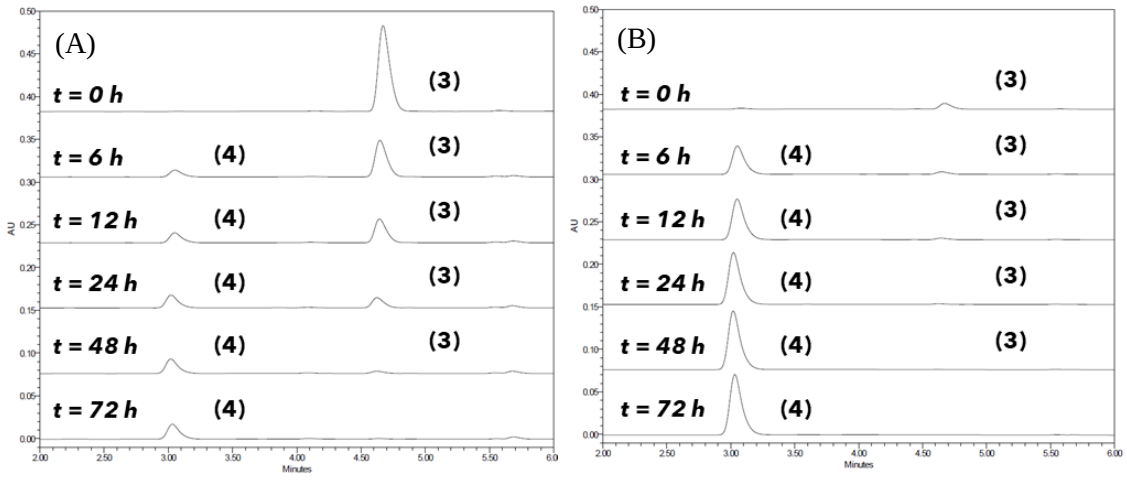

Figure S33: Representative HPLC chromatogram overlay taken at 318 nm (A) and at 380 nm (B) showing the transformation of **PNACAPE** (**3**) to paranitroaniline (**PNA**) (**4**) using palladium loaded C11x3 amphiphilic micelles ([Amphiphile] = 320 µM, [Substrate] = 150 µM, $[Pd(OAc)_2]$ = 75 µM).

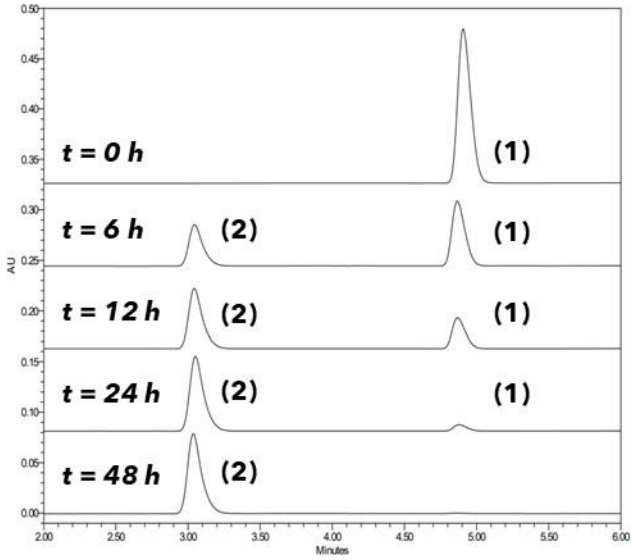

Figure S34: Representative HPLC chromatogram overlay (taken at 307 nm), showing the transformation of **PNPPE** (**1**) to paranitrophenol (**PNP**) (**2**) using palladium loaded C14x3 amphiphilic micelles ([Amphiphile] = 320 µM, [Substrate] = 300 µM, [$Pd(OAc)_2$] = 150 µM).

(A) (B)

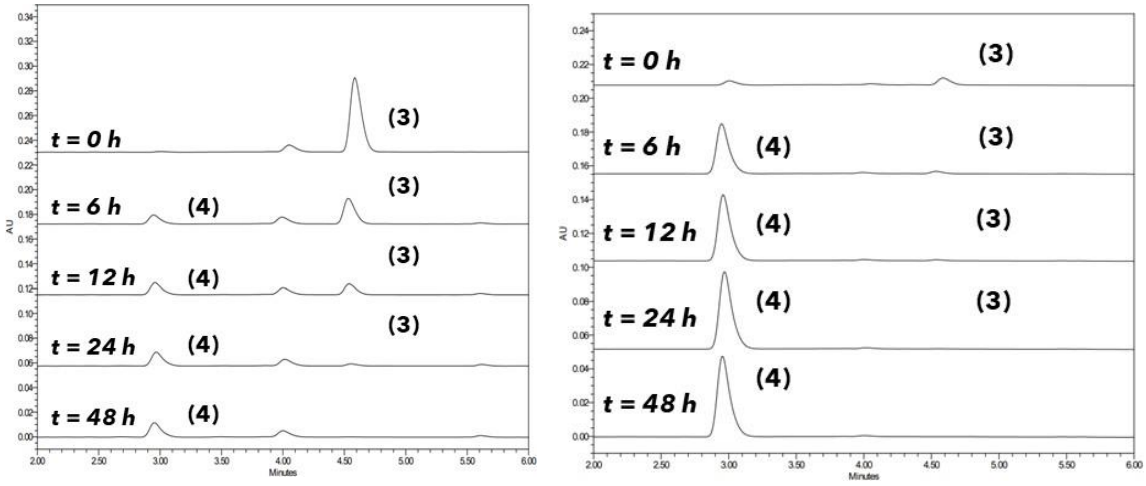

Figure S35: Representative HPLC chromatogram overlay taken at 318 nm (A) and at 380 nm (B) showing the transformation of **PNACAPE** (**3**) to paranitroaniline (**PNA**) (**4**) using palladium loaded C14x3 amphiphilic micelles ([Amphiphile] = 320 µM, [Substrate] = 150 µM, [$Pd(OAc)_2$] = 75 µM).

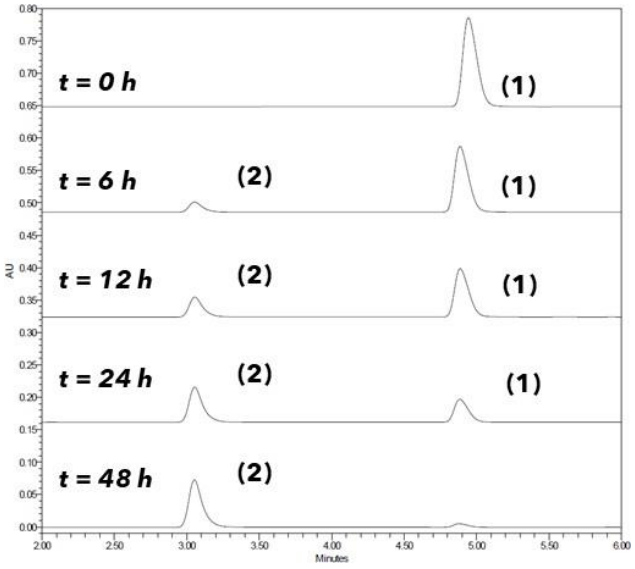

Figure S36: Representative HPLC chromatogram overlay (taken at 307 nm), showing the transformation of **PNPPE** (**1**) to paranitrophenol (**PNP**) (**2**) using palladium loaded C11x4 (3,5) amphiphilic micelles ([Amphiphile] = 320 µM, [Substrate] = 300 µM, [$Pd(OAc)_2$] = 150 µM).

(A) (B)

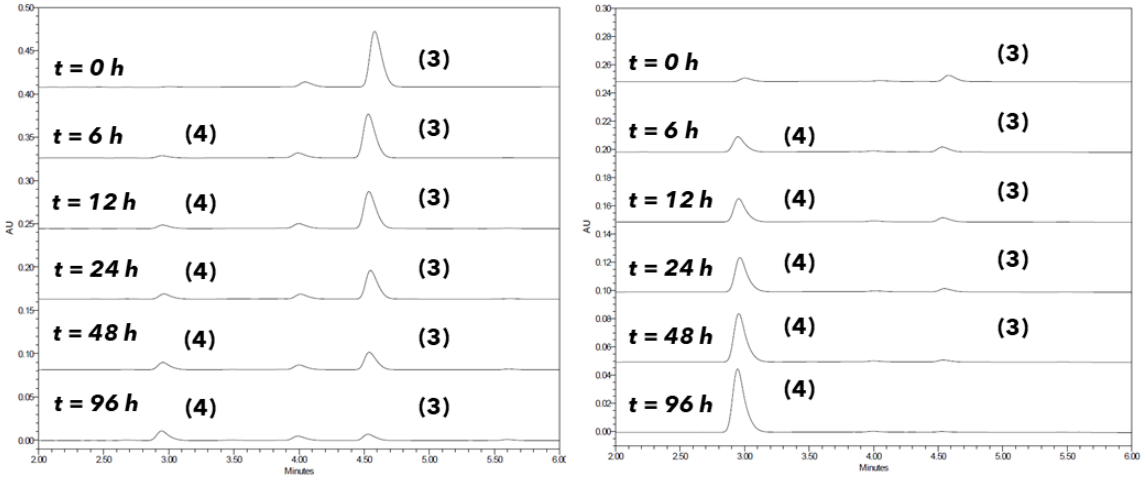

Figure S37: Representative HPLC chromatogram overlay taken at 318 nm (A) and at 380 nm (B) showing the transformation of **PNACAPE** (**3**) to paranitroaniline (**PNA**) (**4**) using palladium loaded C11x4 (3,5) amphiphilic micelles ([Amphiphile] = 320 µM, [Substrate] = 150 µM, [$Pd(OAc)_2$] = 75 µM).

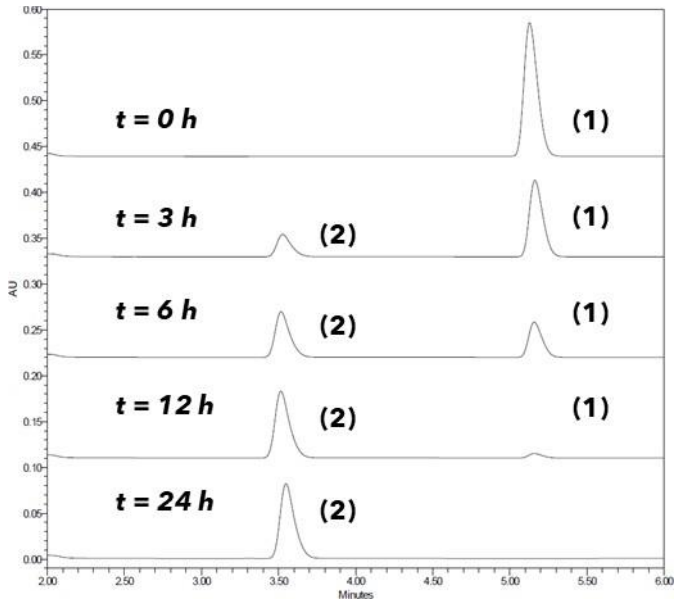

Figure S38: Representative HPLC chromatogram overlay (taken at 307 nm), showing the transformation of **PNPPE** (1) to paranitrophenol (**PNP**) (2) using palladium loaded C11x4 (3,4) amphiphilic micelles ([Amphiphile] = 320 µM, [Substrate] = 300 µM, [$Pd(OAc)_2$] = 150 µM).

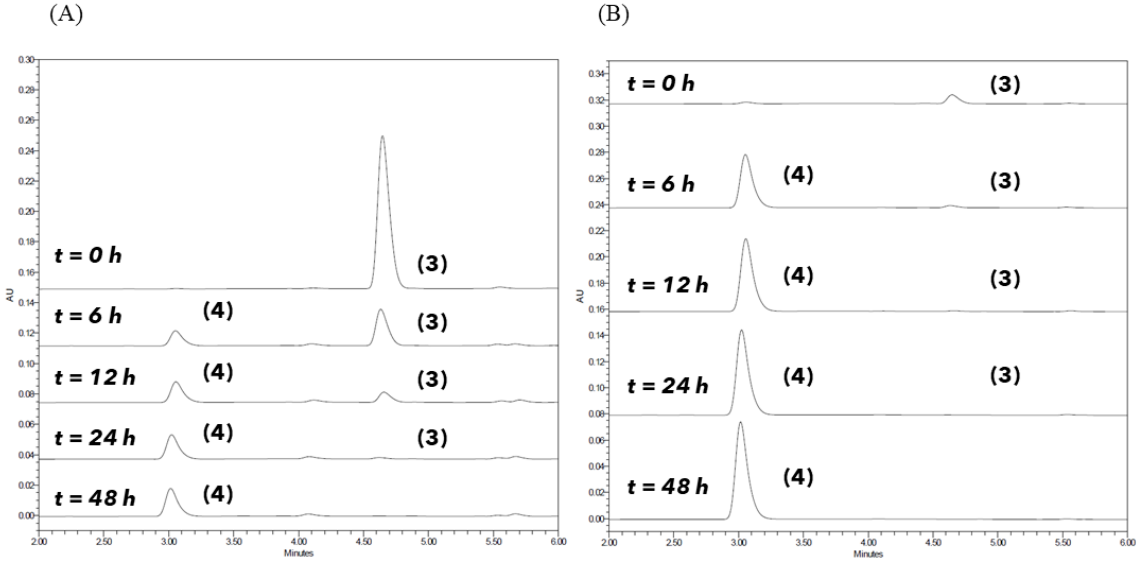

Figure S39: Representative HPLC chromatogram overlay taken at 318 nm (A) and at 380 nm (B) showing the transformation of **PNACAPE** (**3**) to paranitroaniline (**PNA**) (**4**) using palladium loaded C11x4 (3,4) amphiphilic micelles ([Amphiphile] = 320 µM, [Substrate] = 150 µM, [$Pd(OAc)_2$] = 75 µM).

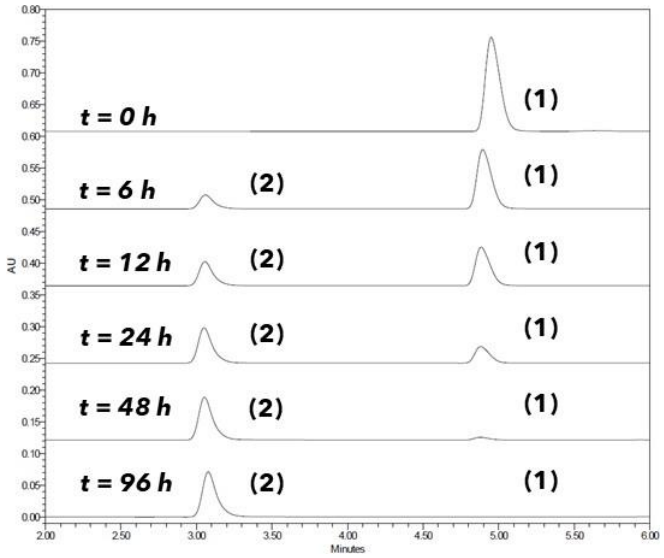

Figure S40: Representative HPLC chromatogram overlay (taken at 307 nm), showing the transformation of **PNPPE** (1) to paranitrophenol (**PNP**) (2) using palladium loaded C6x6 amphiphilic micelles ([Amphiphile] = 320 µM, [Substrate] = 300 µM, [$Pd(OAc)_2$] = 150 µM).

(A) (B)

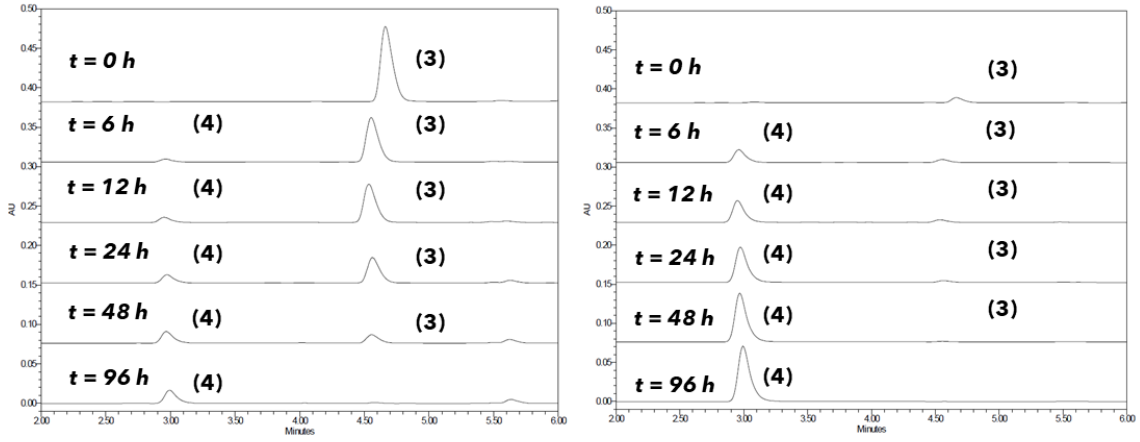

Figure S41: Representative HPLC chromatogram overlay taken at 318 nm (A) and at 380 nm (B) showing the transformation of **PNACAPE** (**3**) to paranitroaniline (**PNA**) (**4**) using palladium loaded C6x6 amphiphilic micelles ([Amphiphile] = 320 µM, [Substrate] = 150 µM, [$Pd(OAc)_2$] = 75 µM).

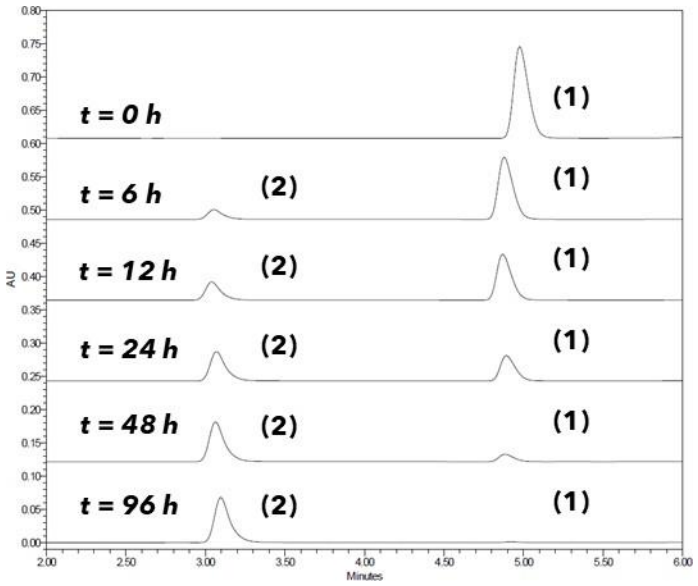

Figure S42: Representative HPLC chromatogram overlay (taken at 307 nm), showing the transformation of **PNPPE** (**1**) to paranitrophenol (**PNP**) (**2**) using palladium loaded C7x6 amphiphilic micelles ([Amphiphile] = 320 µM, [Substrate] = 300 µM, [$Pd(OAc)_2$] = 150 µM).

(A) (B)

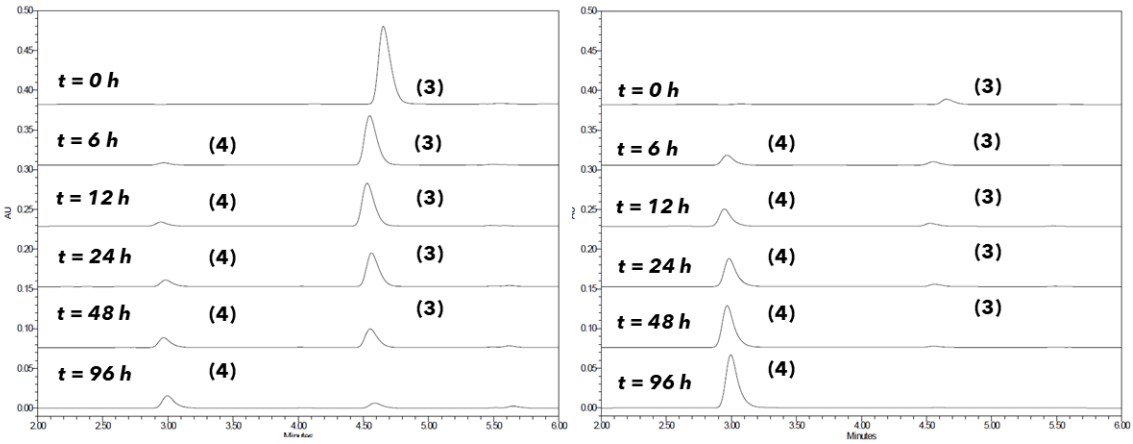

Figure S43: Representative HPLC chromatogram overlay taken at 318 nm (A) and at 380 nm (B) showing the transformation of **PNACAPE** (**3**) to paranitroaniline (**PNA**) (**4**) using palladium loaded C7x6 amphiphilic micelles ([Amphiphile] = 320 µM, [Substrate] = 150 µM, [$Pd(OAc)_2$] = 75 µM).

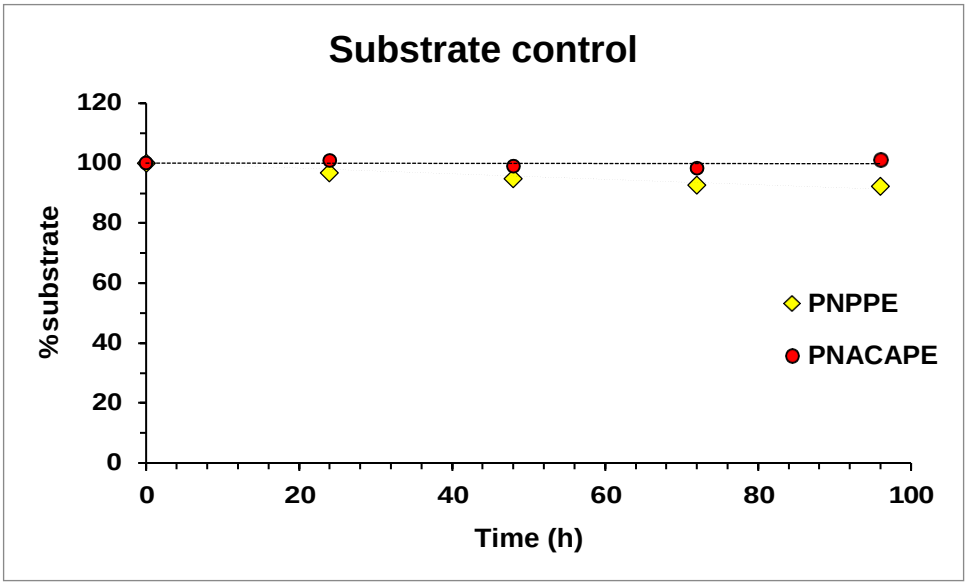

Figure S44*:* Substrate stability in the presence of C11x4 (3,5) amphiphilic micellar solution, without the addition of $Pd(OAc)_2$ salt.

4.2 Inductively coupled plasma mass spectrometry (ICP- MS)

Sample preparation:

The amphiphiles and metal solutions were prepared as described before. $Pd(OAc)_2$ solution in the absence of micelles was prepared by directly dissolving the metal salt in PBS, following by vortex and sonication to afford clear solution.

ICP-MS measurements:

100 µL of the sample solution were mixed with 900 µL of HNO_3 and 200 µL of H_2O_2 and were heated to 95°C for 15 min. The solutions were further diluted with 8.8 mL of water. Measurements were done on 7800 ICP-MS equipped with SPS4 Autosampler (Agilent). The instrument was operated in Helium mode with "General Conditions" plasma. Signal of 105 Pd isotope was measured with 6 replicates per measurement.

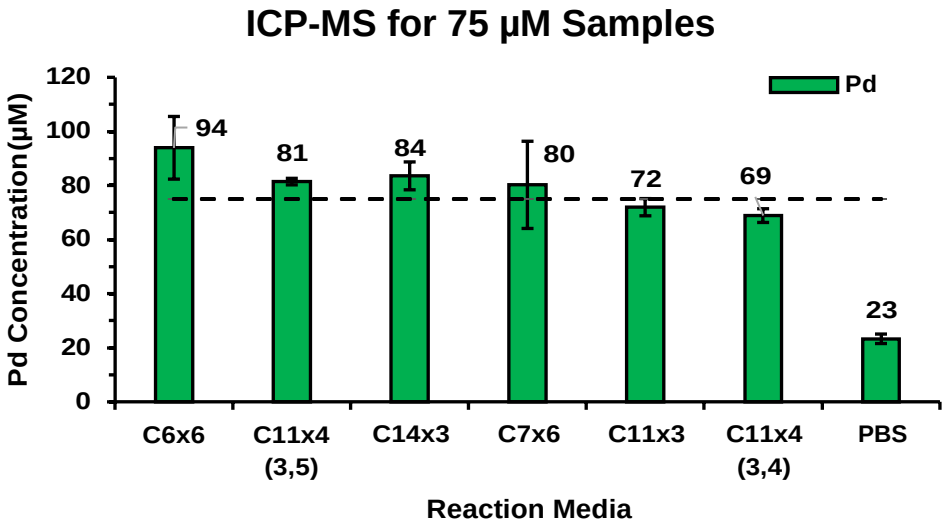

Figure S45: ICP-MS analysis of Pd in the presence of amphiphiles or PBS only, with intended concentration of 75 µM.

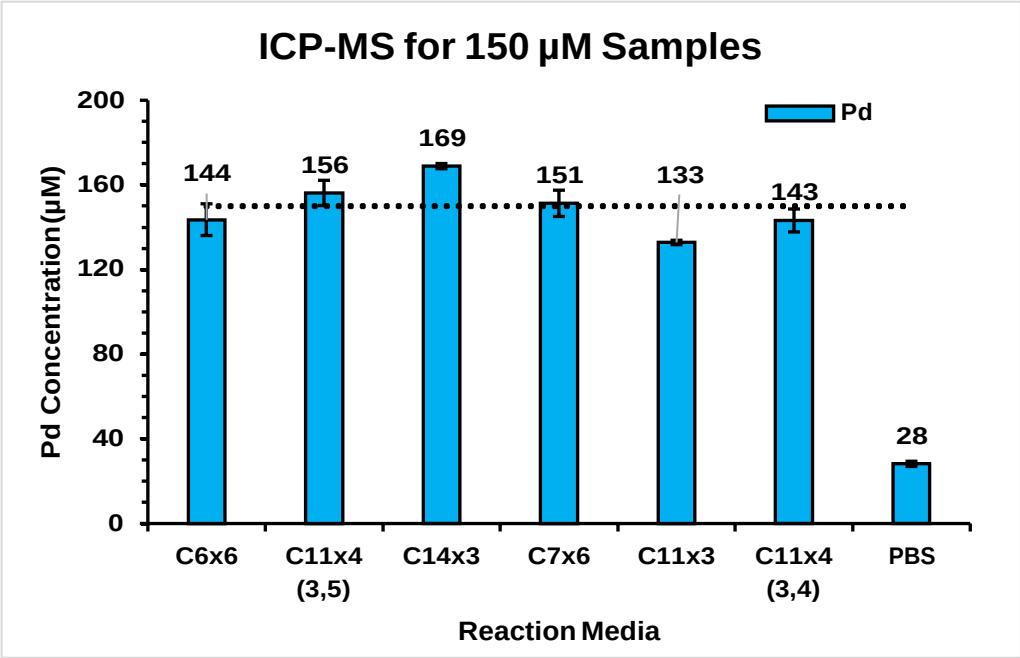

Figure S46: ICP-MS analysis of Pd in the presence of amphiphiles or PBS only, with intended concentration of 150 µM.

***Table S1*:** **A**mphiphiles, substrates and kinetic analysis.

Entry	***Polymer***	***Substrate***	***k (h^{-1})***	***$t_{½}$ cal (h) (=ln2/k)***	***$t_{½}$ exp (h)***
1	C11x3	PNPPE	0.132	5.3	5.3
2		PNACAPE	0.106	6.5	5.8
3	C14x3	PNPPE	0.184	3.8	4.3
4		PNACAPE	0.143	4.9	3.9
5	C11x4 (3,5)	PNPPE	0.066	10.5	10.3
6		PNACAPE	0.052	13.3	16.5
7	C11x4 (3,4)	PNPPE	0.331	2.1	2.5
8		PNACAPE	0.136	5.1	3.5
9	C6x6	PNPPE	0.087	8.0	8.0
10		PNACAPE	0.054	12.9	15.3
11	C7x6	PNPPE	0.101	6.9	7.0
12		PNACAPE	0.068	10.2	10.8

4.3. Anisotropy measurements

Sample preparation:

The amphiphiles and metal solutions were prepared as described before. $Pd(OAc)_2$ solution in the absence of micelles was prepared by directly dissolving the metal salt in ethanol as a system where

the substrate molecules would not show anisotropy, followed by vortex and sonication to afford clear solution.

7.5 µL of Nile red (0.88 mg/mL in Ethanol) was added to 1 mL of solution and the fluorescence was measured in the fluorimeter in presence of light polarizers at the source and at the detector. The measurements were carried out by orienting the polarizers in vertical and horizontal directions having to do 4 measurements per sample.

To determine the anisotropy for each hybrid the maximum emission of Nile Red (at about 630 nm) was plotted for different amphiphiles at different concentrations of palladium acetate. The formula below was used to estimate the anisotropy of the Nile red dye in the core of the amphiphiles with encapsulated palladium:

$$r_s = \frac{I_{VV} - GI_{VH}}{I_{VV} + 2GI_{VH}} \qquad G = \frac{I_{HV}}{I_{HH}}$$

I for intensity

VV denotes vertical polarization at the source and the detector

VH denotes vertical polarization at source and the horizontal polarization detector

HV denotes horizontal polarization at source and vertical polarization at the detector

HH denotes horizontal polarization at source and the detector

G is the grating factor

Excitation: 550 nm

Emission maxima: 630 nm

Step: 5 nm

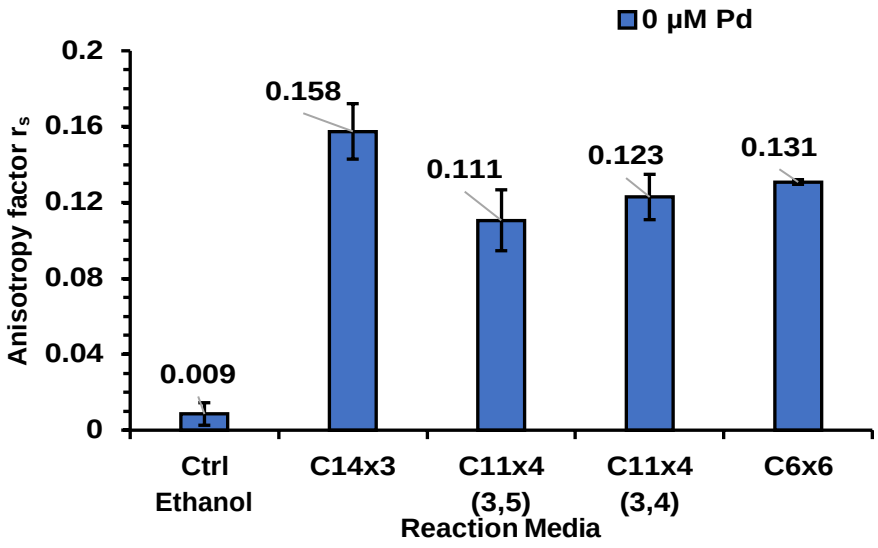

Figure S47: Anisotropy factor for Nile Red molecule in presence of micelles ([amphiphile]=320 µM) with no encapsulated palladium acetate.

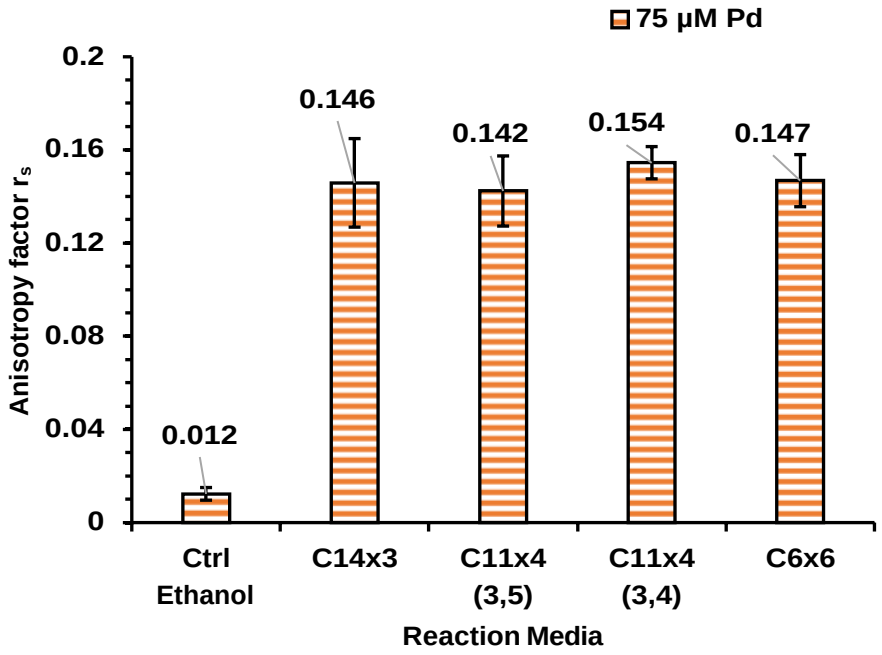

Figure S48: Anisotropy factor for Nile Red molecule in presence of micelles ([amphiphile]=320 µM) and control with encapsulated palladium acetate [75 µM].

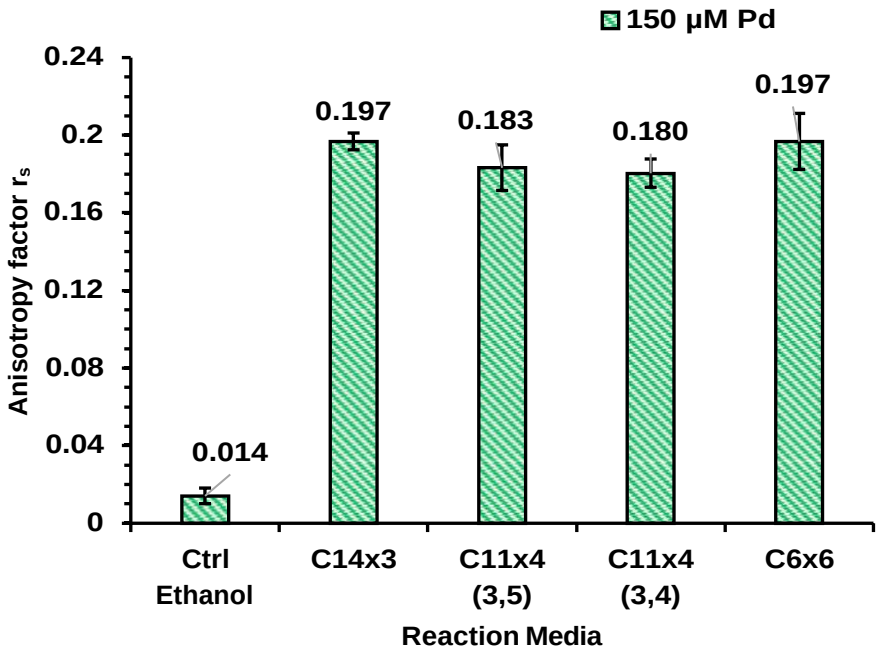

Figure S49: Anisotropy factor for Nile Red molecule in presence of micelles ([amphiphile]=320 µM) and control with encapsulated palladium acetate [150 µM].

5. DFT Computations:

DFT calculations were performed using Gaussian 09.2.[4] Geometry optimization of all the molecules were carried out using the BP86-D3 method[5–12] with Ahlrichs' def2-SVP basis set,[13] and with the relativistic effect of Pd, which was accounted for by the Stuttgart-Dresden ECP,[14,15] implemented in the Gaussian 09 software. Thermal energy corrections were extracted from the results of frequency analysis performed at the same level of theory. Frequency analysis of all the molecules and intermediates contained no imaginary frequency showing that these are energy minima.

Optimized geometries

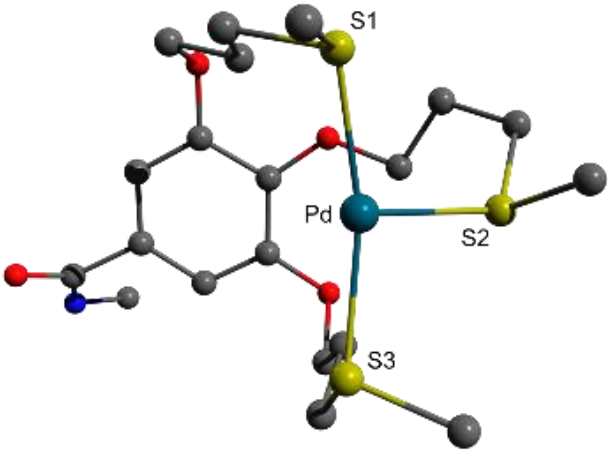

Figure S50: Predicted Geometry for three-armed architecture.

C	3.84994	1.43626	-0.20723
C	4.40728	0.13706	-0.31173
C	3.75220	-0.95397	0.28238
C	2.57998	-0.76469	1.03988
C	2.07576	0.56478	1.25865
C	2.71443	1.65702	0.57085
O	2.18462	2.91235	0.68433
O	1.02417	0.92030	2.01679

O	1.90568	-1.83315	1.57049
C	5.57665	-0.05410	-1.24579
N	6.70133	-0.67431	-0.83118
O	5.39186	0.36156	-2.40350
C	7.07184	-1.04643	0.53209
C	1.29851	3.32457	-0.37466
S	-2.76124	2.24117	-0.58314
C	-0.02379	0.04849	2.47609
C	-1.23381	0.94168	2.76471
C	-2.57037	0.21505	2.86232
S	-2.97644	-0.85896	1.38306
C	1.46414	-2.84081	0.62814
C	0.11874	-2.36491	0.05298
C	-0.38986	-3.03916	-1.21781
S	-1.98706	-2.25413	-1.76636
C	-4.79603	-0.65743	1.35782
C	-3.22827	-3.40386	-1.07265
C	-3.85812	2.60104	-2.00952
C	-0.07281	2.66600	-0.16746
C	-1.18411	3.06434	-1.13447
H	4.30687	2.28346	-0.73883
H	4.15719	-1.97159	0.17828
H	7.40575	-0.80037	-1.56850
H	6.35220	-0.61572	1.25348

H	8.07731	-0.64580	0.77220
H	7.09212	-2.14905	0.66104
H	1.73260	3.07161	-1.36973
H	1.23120	4.42819	-0.29602
H	0.31434	-0.53060	3.36102
H	-0.27278	-0.67399	1.67872
H	-1.08393	1.51356	3.70500
H	-1.30801	1.68995	1.95332
H	-3.39778	0.94400	2.97259
H	-2.61879	-0.49859	3.71366
H	1.36579	-3.78222	1.20283
H	2.21692	-2.99692	-0.17425
H	0.23686	-1.28092	-0.17540
H	-0.65231	-2.44866	0.84601
H	-0.59458	-4.12316	-1.10213
H	0.30608	-2.90915	-2.07211
H	-5.19213	-1.30406	0.55211
H	-5.06806	0.40063	1.17534
H	-5.19319	-0.99743	2.33586
H	-4.22367	-2.99209	-1.32757
H	-3.10939	-3.48271	0.02730
H	-3.10833	-4.39416	-1.55408
H	-4.83311	2.11816	-1.80672
H	-3.42602	2.21514	-2.95364

H	-3.99688	3.69940	-2.06661
H	-0.37215	2.90613	0.87232
H	0.05639	1.56130	-0.21449
H	-0.98164	2.75891	-2.18255
H	-1.39659	4.15450	-1.11543
Pd	-2.31957	-0.09893	-0.79813

Sum of electronic and zero-point Energies= -2458.211114

Sum of electronic and thermal Energies= -2458.175595

Sum of electronic and thermal Enthalpies= -2458.174651

Sum of electronic and thermal Free Energies= -2458.279022

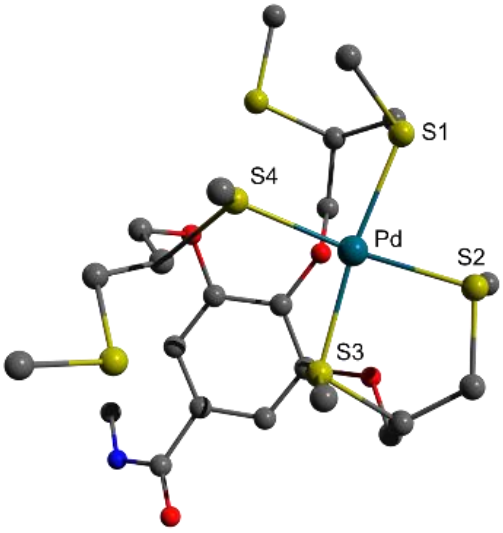

Figure S51: Predicted geometry for six-armed architecture.

C	2.87318	0.98940	-1.91322
C	3.60674	-0.16449	-1.58060
C	2.92844	-1.34745	-1.23062
C	1.52297	-1.36883	-1.24443

C	0.78361	-0.24420	-1.67958
C	1.47212	0.96323	-1.94255
O	0.70067	2.09222	-2.16631
O	-0.59531	-0.27923	-1.67454
O	0.78071	-2.42483	-0.76049
C	5.10521	0.02383	-1.40188
N	5.94623	-0.96639	-1.82324
O	5.49743	1.05669	-0.85237
C	5.67089	-2.10101	-2.69712
C	1.11037	3.28810	-1.50086
C	0.43769	3.52257	-0.12793
S	0.55366	1.97454	0.94889
C	-0.98372	4.07413	-0.12586
S	-2.33860	2.85442	-0.42914
C	-1.21872	-1.11114	-2.67991
C	-2.49220	-1.80678	-2.18859
S	-2.13882	-3.22417	-1.05447
C	-3.62812	-0.87466	-1.72776
S	-3.63892	-0.03743	-0.07245
C	1.07289	-2.79161	0.59001
C	0.93852	-1.59881	1.56533
S	-0.89751	-1.15481	1.65091
C	1.58211	-1.86007	2.93361
S	2.17840	-0.27890	3.66237

C	-2.31339	2.64577	-2.24848
C	0.33997	2.71219	2.61282
C	-4.14831	-1.36521	1.07244
C	-3.67211	-4.19130	-1.30158
C	2.73725	-0.87024	5.29791
C	-1.22917	-0.74662	3.41126
H	3.43520	1.91396	-2.10860
H	3.48336	-2.23615	-0.89693
H	6.92873	-0.76613	-1.60460
H	5.64044	-3.06542	-2.14348
H	6.46017	-2.17890	-3.47200
H	4.70516	-1.96343	-3.21982
H	0.84634	4.13811	-2.16418
H	2.20905	3.30980	-1.35956
H	-1.10623	4.89097	-0.86876
H	-1.24303	4.50157	0.86385
H	-1.47798	-0.45723	-3.54442
H	-0.50140	-1.88157	-3.03083
H	-2.89555	-2.27602	-3.11669
H	-3.74880	-0.03668	-2.44655
H	-4.59527	-1.41938	-1.72376
H	2.11022	-3.18620	0.68052
H	0.37239	-3.61395	0.83854
H	1.44032	-0.72532	1.09334

H	2.45975	-2.52565	2.78479
H	0.90111	-2.38997	3.63384
H	-3.21979	2.06351	-2.49819
H	-1.38721	2.12667	-2.55771
H	-2.40249	3.65015	-2.70759
H	1.14705	3.45651	2.76280
H	0.49202	1.87673	3.32407
H	-0.65954	3.16669	2.74325
H	-5.14412	-1.71906	0.73964
H	-4.24926	-0.89665	2.07028
H	-3.40831	-2.18871	1.06334
H	-3.53562	-5.13172	-0.73191
H	-3.81421	-4.44891	-2.37096
H	-4.57624	-3.67893	-0.91202
H	3.13921	0.01376	5.83036
H	3.54859	-1.61667	5.18422
H	1.89783	-1.29709	5.88288
H	-1.41019	-1.69213	3.95764
H	-2.15053	-0.13434	3.42076
H	-0.38230	-0.18800	3.85903
Pd	-1.46848	0.84248	0.48001
H	1.08120	4.25817	0.40529

Sum of electronic and zero-point Energies= -3770.401421

Sum of electronic and thermal Energies= -3770.357744

Sum of electronic and thermal Enthalpies= -3770.356800

Sum of electronic and thermal Free Energies= -3770.477487

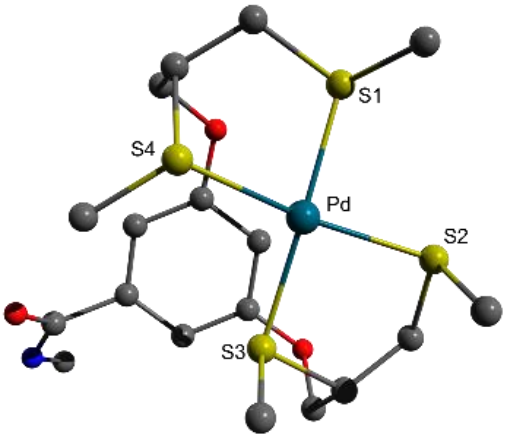

Figure S52: Predicted geometry for four-armed (3,5) architecture.

C	-3.01313	0.97805	0.74549
C	-3.28249	-0.35464	0.39884
C	-2.38440	-1.38279	0.75301
C	-1.18877	-1.07788	1.41539
C	-0.90953	0.25794	1.78876
C	-1.81422	1.27274	1.42282
C	-4.35195	-0.72705	-0.60880
N	-5.63636	-0.35162	-0.39924
O	-3.96556	-1.33585	-1.62127
C	-6.23091	0.21496	0.80806
O	-1.46963	2.58751	1.69806
O	-0.20586	-2.00879	1.69471

C	-1.26399	3.41821	0.56062
C	-0.16154	-3.22731	0.95907
C	0.95051	-3.24336	-0.10569
C	2.37743	-3.11690	0.43097
S	0.84434	-1.94638	-1.45715
S	2.71309	-1.41711	1.11260
C	0.06365	3.08550	-0.17435
C	1.20331	3.05410	0.85440
S	2.59030	1.88868	0.57836
S	-0.15079	1.47105	-1.17375
C	-0.84576	-2.05328	-2.13167
C	4.49207	-1.24885	0.71012
C	3.50349	2.64555	-0.81519
C	0.32618	2.01343	-2.85876
H	-3.70164	1.78637	0.45976
H	-2.64307	-2.40543	0.44988
H	0.00173	0.49313	2.35665
H	-6.26675	-0.59484	-1.17268
H	-5.52160	0.14289	1.65405
H	-7.14391	-0.35128	1.08215
H	-6.51218	1.28054	0.66790
H	-1.19419	4.45633	0.94801
H	-2.11523	3.38439	-0.15562
H	-1.12916	-3.47783	0.48323

H	0.06077	-4.04172	1.68217
H	3.12276	-3.31479	-0.36653
H	2.54939	-3.82985	1.26425
H	0.24127	3.85172	-0.95667
H	0.79969	2.73963	1.83869
H	1.64871	4.06302	0.98345
H	-1.06410	-3.12573	-2.30842
H	-0.80401	-1.54094	-3.11237
H	-1.63396	-1.59877	-1.49721
H	4.80572	-0.25042	1.07281
H	4.66891	-1.34959	-0.37812
H	5.04633	-2.02500	1.27486
H	4.28630	1.92528	-1.12149
H	3.98140	3.57240	-0.43896
H	2.84030	2.86928	-1.67027
H	0.23555	1.12233	-3.50983
H	1.36002	2.40399	-2.90198
H	-0.39996	2.78064	-3.19378
Pd	1.46555	0.01684	-0.30525
H	0.87804	-4.21237	-0.64942

Sum of electronic and zero-point Energies= -2702.726134

Sum of electronic and thermal Energies= -2702.693941

Sum of electronic and thermal Enthalpies= -2702.692997

Sum of electronic and thermal Free Energies= -2702.78740

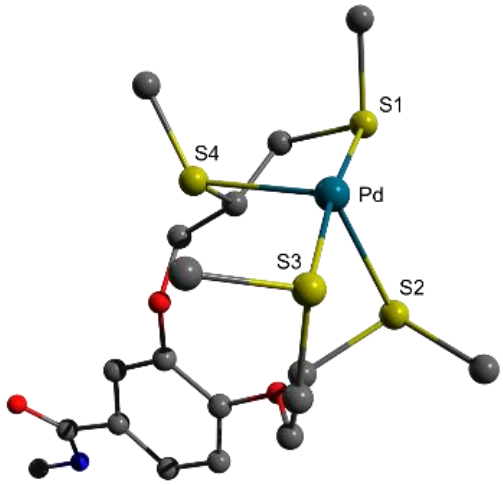

Figure S53: Predicted geometry for four-armed (3,4) architecture.

C	-5.06505	0.10627	0.02769
C	-4.90818	1.33465	0.70275
C	-3.62394	1.81026	1.01592
C	-2.48348	1.07476	0.64970
C	-2.63720	-0.14163	-0.06951
C	-3.92069	-0.61586	-0.36912
O	-1.51649	-0.80563	-0.54642
O	-1.21931	1.49424	1.03154
C	-6.40170	-0.46347	-0.39221
O	-6.46472	-1.26252	-1.33647
N	-7.50675	-0.06346	0.30594
C	-8.84318	-0.55126	-0.00791
C	-0.59781	2.56226	0.30280
C	0.76279	2.00439	-0.13849
C	-1.05149	-1.96488	0.15391
C	0.43556	-1.68864	0.42172

C	1.21870	-2.53402	1.41826
S	2.85899	-1.68276	1.77212
S	1.38261	-1.50326	-1.19747
C	1.56628	2.70065	-1.22807
S	1.85178	1.63448	1.36213
S	3.10149	1.68610	-1.62485
C	2.68348	1.04942	-3.28695
C	2.75462	3.20144	1.63718
C	1.76536	-3.22880	-1.66191
C	4.09949	-2.96990	1.39483
H	-5.78162	1.94625	0.97715
H	-3.49279	2.75322	1.56837
H	-4.04694	-1.54065	-0.95229
H	-7.37257	0.43134	1.19152
H	-8.86331	-0.86716	-1.06808
H	-9.58441	0.25415	0.16308
H	-9.11754	-1.42755	0.61956
H	-0.50805	3.46770	0.94372
H	-1.19099	2.83524	-0.59934
H	0.50126	0.99190	-0.50798
H	-1.22385	-2.88246	-0.45227
H	-1.57736	-2.09209	1.12704
H	0.41128	-0.64661	0.80335
H	1.41862	-3.57170	1.08401

H	0.68996	-2.58228	2.39274
H	1.91491	3.71722	-0.95692
H	0.97967	2.78081	-2.16608
H	3.49764	0.35365	-3.56870
H	2.67211	1.90353	-3.99311
H	1.70790	0.52505	-3.27468
H	2.02142	4.02158	1.77573
H	3.46369	3.43211	0.81898
H	3.31638	3.05682	2.58074
H	2.42861	-3.73198	-0.93405
H	2.26849	-3.17546	-2.64682
H	0.81331	-3.78648	-1.77245
H	5.08552	-2.52261	1.62914
H	4.06575	-3.27520	0.33124
H	3.92498	-3.83460	2.06621
Pd	2.95848	-0.08185	-0.02011

Sum of electronic and zero-point Energies= -2702.665766

Sum of electronic and thermal Energies= -2702.632302

Sum of electronic and thermal Enthalpies= -2702.631358

Sum of electronic and thermal Free Energies= -2702.731756

6. References

(1) Harnoy, A. J.; Buzhor, M.; Tirosh, E.; Shaharabani, R.; Beck, R.; Amir, R. J. Modular Synthetic Approach for Adjusting the Disassembly Rates of Enzyme-Responsive Polymeric Micelles. *Biomacromolecules* **2017**, *18* (4), 1218–1228. https://doi.org/10.1021/acs.biomac.6b01906.

(2) Tevet, S.; Wagle, S. S.; Slor, G.; Amir, R. J. Tuning the Reactivity of Micellar Nanoreactors by Precise Adjustments of the Amphiphile and Substrate Hydrophobicity. *Macromolecules* **2021**. https://doi.org/10.1021/acs.macromol.1c01755.

(3) Ramesh, R.; Chandrasekaran, Y.; Megha, R.; Chandrasekaran, S. Base Catalyzed Cyclization of N-Aryl and N-Alkyl-O-Propargyl Carbamates to 4-Alkylidene-2-Oxazolidinones. *Tetrahedron* **2007**, *63* (37), 9153–9162. https://doi.org/https://doi.org/10.1016/j.tet.2007.06.066.

(4) Frisch, M. J.; Trucks, G. W.; Schlegel, H. B.; Scuseria, G. E.; Robb, M. A.; Cheeseman, J. R.; Scalmani, G.; Barone, V.; Mennucci, B.; Petersson, G. A.; Nakatsuji, H.; Caricato, M.; Li, X.; Hratchian, H. P.; Izmaylov, A. F.; Bloino, J.; Zheng, G.; Sonnenberg, J. L.; Hada, M.; Ehara, M.; Toyota, K.; Fukuda, R.; Hasegawa, J.; Ishida, M.; Nakajima, T.; Honda, Y.; Kitao, O.; Nakai, H.; Vreven, T.; Montgomery, Jr., J. A.; Peralta, J. E.; Ogliaro, F.; Bearpark, M.; Heyd, J. J.; Brothers, E.; Kudin, K. N.; Staroverov, V. N.; Keith, T.; Kobayashi, R.; Normand, J.; Raghavachari, K.; Rendell, A.; Burant, J. C.; Iyengar, S. S.; Tomasi, J.; Cossi, M.; Rega, N.; Millam, J. M.; Klene, M.; Knox, J. E.; Cross, J. B.; Bakken, V.; Adamo, C.; Jaramillo, J.; Gomperts, R.; Stratmann, R. E.; Yazyev, O.; Austin, A. J.; Cammi, R.; Pomelli, C.; Ochterski, J. W.; Martin, R. L.; Morokuma, K.; Zakrzewski, V. G.; Voth, G. A.; Salvador, P.; Dannenberg, J. J.; Dapprich, S.; Daniels, A. D.; Farkas, O.; Foresman, J. B.; Ortiz, J. V.; Cioslowski, J.; Fox, D. J. Gaussian 09, Revision D. 01. *Gaussian, Inc., Wallingford CT* **2013**.

(5) Weigend, F.; Ahlrichs, R. Balanced Basis Sets of Split Valence, Triple Zeta Valence and Quadruple Zeta Valence Quality for H to Rn: Design and Assessment of Accuracy. *Phys. Chem. Chem. Phys.* **2005**, *7* (18), 3297–3305. https://doi.org/10.1039/B508541A.

(6) Chai, J.-D.; Head-Gordon, M. Long-Range Corrected Hybrid Density Functionals with Damped Atom–Atom Dispersion Corrections. *Phys. Chem. Chem. Phys.* **2008**, *10* (44),

6615–6620. https://doi.org/10.1039/B810189B.

(7) Chai, J.-D.; Head-Gordon, M. Systematic Optimization of Long-Range Corrected Hybrid Density Functionals. *J. Chem. Phys.* **2008**, *128* (8), 84106. https://doi.org/10.1063/1.2834918.

(8) Grimme, S. Accurate Calculation of the Heats of Formation for Large Main Group Compounds with Spin-Component Scaled MP2 Methods. *J. Phys. Chem. A* **2005**, *109* (13), 3067–3077. https://doi.org/10.1021/jp050036j.

(9) Quintal, M. M.; Karton, A.; Iron, M. A.; Boese, A. D.; Martin, J. M. L. Benchmark Study of DFT Functionals for Late-Transition-Metal Reactions. *J. Phys. Chem. A* **2006**, *110* (2), 709–716. https://doi.org/10.1021/jp054449w.

(10) Li, Q. S.; Zhang, J.; Zhang, S. A DFT and Ab Initio Direct Dynamics Study on the Hydrogen Abstract Reaction of H3BNH3→H2+H2BNH2. *Chem. Phys. Lett.* **2005**, *404* (1), 100–106. https://doi.org/https://doi.org/10.1016/j.cplett.2005.01.024.

(11) Grimme, S.; Antony, J.; Ehrlich, S.; Krieg, H. A Consistent and Accurate Ab Initio Parametrization of Density Functional Dispersion Correction (DFT-D) for the 94 Elements H-Pu. *J. Chem. Phys.* **2010**, *132* (15), 154104. https://doi.org/10.1063/1.3382344.

(12) Pantazis, D. A.; Neese, F. All-Electron Scalar Relativistic Basis Sets for the 6p Elements. *Theor. Chem. Acc.* **2012**, *131* (11), 1292. https://doi.org/10.1007/s00214-012-1292-x.

(13) Schwerdtfeger, P.; Dolg, M.; Schwarz, W. H. E.; Bowmaker, G. A.; Boyd, P. D. W. Relativistic Effects in Gold Chemistry. I. Diatomic Gold Compounds. *J. Chem. Phys.* **1989**, *91* (3), 1762–1774. https://doi.org/10.1063/1.457082.

(14) Wedig, U.; Dolg, M.; Stoll, H.; Preuss, H. Energy-Adjusted Pseudopotentials for Transition-Metal Elements. In *Quantum Chemistry: The Challenge of Transition Metals and Coordination Chemistry*; Veillard, A., Ed.; 1986; pp 79–89.

(15) Andrae, D.; Häußermann, U.; Dolg, M.; Stoll, H.; Preuß, H. Energy-Adjustedab Initio Pseudopotentials for the Second and Third Row Transition Elements. *Theor. Chim. Acta* **1990**, *77* (2), 123–141. https://doi.org/10.1007/BF01114537.